

1 **Sensitivity of high-temperature weather to initial soil moisture:**
2 **A case study using the WRF model**

3 **X.-M. Zeng^{1,2}, B. Wang^{1,2}, Y. Zhang¹, S. Song¹, X. Huang¹, Y. Zheng¹, C. Chen¹,**
4 **and G. Wang^{1,2}**

5 [1] College of Meteorology and Oceanography, PLA University of Science and Technology,
6 Nanjing, Jiangsu, China

7 [2] Key Laboratory for Mesoscale Severe Weather of Ministry of Education, Nanjing
8 University, Nanjing, Jiangsu, China

9 Correspondence to: X.-M. Zeng (zen_xm@yahoo.com)

10
11 **Abstract**

12 Using a succession of 24-hour Weather Research and Forecasting model (WRF) simulations,
13 we investigate the sensitivity to initial soil moisture of a short-range high-temperature weather
14 event that occurred in late July 2003 in East China. The initial soil moisture (SMOIS) in the
15 Noah land surface scheme is adjusted [relative to the control run (CTL)] for four groups of
16 simulations: DRY25 (-25%), DRY50 (-50%), WET25 (+25%) and WET50 (+50%). Ten 24-
17 hour integrations are performed in each group.

18 We focus on 2-m surface air temperature (SAT) greater than 35°C (the threshold of “high
19 temperature” events in China) at 0600 UTC (roughly 1400 LT in the study domain) to analyse
20 the occurrence of the high-temperature event. The ten-day mean results show that the 0600
21 UTC SAT (SAT06) is sensitive to the SMOIS change; specifically, SAT06 exhibits an
22 apparent increase with the SMOIS decrease (e.g., compared with CTL, DRY25 generally
23 results in a 1°C SAT06 increase over the land surface of East China), areas with 35°C or
24 higher SAT06 are the most affected, and the simulations are more sensitive to the SMOIS
25 decrease than to the SMOIS increase, which suggests that hot weather can be amplified under
26 low soil moisture conditions. Regarding the mechanism underlying the extremely high SAT06,
27 sensible heat flux has been shown to directly heat the lower atmosphere, and latent heat flux
28 has been found to be more sensitive to the SMOIS change, resulting in an overall increase in
29 surface net radiation due to the increased greenhouse effect (e.g., with the SMOIS increase
30 from DRY25 to CTL, the ten-day mean net radiation increases by 5 W m⁻²). Additionally, due

1 to the unique and dynamic nature of the western Pacific subtropical high, negative feedback
2 occurs between the regional atmospheric circulation and the air temperature in the lower
3 atmosphere while positive feedback occurs in the mid-troposphere.

4 Using a method based on an analogous temperature relationship, a detailed analysis of the
5 physical processes shows that for the SAT change, the SMOIS change affects diabatic
6 processes (e.g., surface fluxes) more strongly than the adiabatic process of subsidence in the
7 western Pacific subtropical high in the five groups of simulations. Interestingly, although
8 diabatic processes dominate subsidence during the daytime and nighttime separately, they do
9 not necessarily dominate during the 24-hour periods (e.g., they are dominant in the WET and
10 CTL simulations only). Further, as the SMOIS decreases, the SAT06 increases, which is
11 largely due to the reduced cooling effect of the diabatic processes, rather than the warming
12 effect of subsidence.

13 Unlike previous studies on heatwave events at climate time scales, this paper presents the
14 sensitivity of simulated short-term hot weather to initial soil moisture and emphasises the
15 importance of appropriate soil moisture initialization when simulating hot weather.

16

17 **1 Introduction**

18 Under the background of global warming, heat wave events have occurred frequently
19 worldwide, especially in the early twenty-first century. As stated in a report by the World
20 Meteorological Organisation, the first decade of the century was the hottest on record since
21 modern measurements began circa 1850 (WMO, 2013). In the summer of 2003, Continental
22 Europe was hit by a persistent abnormal heat wave during which the average summer
23 temperature in most areas was 3°C higher than that of the 30-year (1961-1969) average; over
24 35,000 heat-related deaths were estimated across Europe (e.g., Larsen, 2003). In the same
25 period, abnormal high-temperature weather also occurred in the regions south of the Yangtze
26 River and South China (e.g., Lin et al., 2005; Yang and Li, 2005; Zeng et al., 2011), resulting
27 in increased daily mortalities (Tan et al., 2007). In the summer of 2010, persistent and
28 abnormally hot weather occurred in Eastern Europe and Russia, during which the maximum
29 average regional temperature in western Russia was 8-10°C higher than the average summer
30 temperature for the period of 2003-2009; the super heat wave events in 2003 and 2010 likely
31 surpassed the maximum summer temperature of the last 500 years over nearly half of Europe
32 (Barriopedro et al., 2011; Lau and Kim, 2012). In early July 2012, over half of America was

1 hit by a persistent heat wave for approximately one week, and record-high temperatures were
2 set in many places (Donat et al., 2013). These high temperature and heat wave events not only
3 directly threaten human health and safety but also cause droughts and forest fires, which pose
4 serious hazards to the entire ecological system and severely impact electrical power,
5 transportation, etc. (Tan et al., 2007; Zeng et al., 2011).

6 In recent decades, researchers have investigated the causes of the formation and persistence of
7 high-temperature and heat wave events from various aspects (e.g., Wolfson et al., 1987; Lyon
8 and Dole, 1995; Lin et al., 2005; Fischer et al., 2007; Zeng et al., 2011; Lau and Kim, 2012).
9 Land-atmosphere interactions are known to have an important impact on weather and climate
10 (e.g., Shukla and Mintz, 1982; Pielke, 2001; Koster et al., 2004; Guo et al. 2011). Specifically,
11 the influence of soil moisture anomalies on high-temperature events has been widely
12 investigated (Wolfson et al., 1987; Ferranti and Viterbo, 2006; Fischer et al., 2007; Fennessy
13 and Kinter, 2011; Lau and Kim, 2012). For example, Wolfson et al. (1987) used a series of
14 general circulation model experiments to explore the roles of sea surface temperature
15 anomalies of the North Pacific, soil moisture anomalies of the American continent and solar
16 radiative forcing in the maintenance and weakening of the extreme heat wave of the United
17 States in the summer of 1980; in the case of a warm and dry environment, low soil moisture
18 was beneficial for the maintenance of the event. In studying the 2003 heat wave in Europe,
19 Fischer et al. (2007) indicated that during the heat wave, the soil moisture was extremely low,
20 which substantially reduced latent cooling (latent heat flux) and greatly increased the surface
21 temperature anomaly; their regional climate model sensitivity simulations showed that soil
22 moisture played a key role in the partitioning of net radiation into latent and sensible heat
23 fluxes and in the evolution of the heat wave. Positive feedback was identified between soil
24 moisture, atmospheric circulation, and temperature based on the summer anomalies of
25 geopotential heights and air temperature in the troposphere. Hirschi et al. (2011) analysed
26 observational indices and found a relationship between soil-moisture deficit and summer hot
27 extremes in southeastern Europe; the results were compared with climate model simulations.
28 Using an atmospheric general circulation model, Fennessy and Kinter (2011) emphasised the
29 important roles of both the warm local sea surface temperature and the dry local soil in
30 intensifying the 2003 European heat wave. Using two long-term Weather Research and
31 Forecasting model (WRF) simulations with and without soil moisture-atmosphere interactions
32 to evaluate the influence of the land-atmosphere coupling on a summer heat wave in China,
33 Zhang and Wu (2011) found that the land-atmosphere coupling amplifies hot extremes over

1 China, especially in most areas of eastern and southeastern China; the increase was
2 statistically significant. Regarding the summer 2010 Russian heat wave, Lau and Kim (2012)
3 demonstrated that there was positive feedback between the extratropical atmospheric blocking
4 pattern and an underlying extensive land region with below-normal soil moisture, which
5 amplified the heat wave. In most of these investigations, weather or climate models were used
6 for continuous integration for a relatively long time (e.g., seasons) to explore the influence of
7 soil moisture on the heat wave events. It was concluded that the precedent low soil moisture
8 or low soil moisture during the events was beneficial for the generation, maintenance or
9 enhancement of heat waves.

10 There have been many numerical studies concerning the effect of different land surface
11 schemes or initial model conditions on short-range weather (e.g., Xue et al., 2001; Holt et al.,
12 2006; Lei et al., 2008; Sun et al., 2012). Many of these studies highlighted the importance of
13 land surface processes on heavy rainfall events. However, there has been relatively little
14 research focusing on the role of soil moisture in the formation or development of high-
15 temperature weather at short time scales (e.g., 24 hours). This research is important for two
16 reasons. First, soil moisture is a key physical quantity in land-atmosphere interactions, e.g., in
17 the Global Land Atmosphere Coupling Experiment (GLACE), soil moisture-precipitation
18 coupling strength and soil moisture initialisation in numerical models were the research
19 focuses in the two phases of the project (Koster et al., 2006; Guo et al., 2011) (these were also
20 focuses in the mentioned literature). Second, the role of soil moisture might differ at different
21 timescales and affect simulation results. In this regard, relatively long-term soil moisture
22 effects have received attention. For example, observations have shown that in many areas, soil
23 moisture anomalies can persist for weeks to months (e.g., Vinnikov and Yeserkepova, 1990;
24 Seneviratne et al., 2006), and a large number of studies have quantified the effect of soil
25 moisture initialisation on the performance of sub-seasonal to seasonal climatology forecasts.
26 Soil moisture anomalies and soil moisture differences have been shown to impact climate
27 variability and even substantially affect forecast accuracy by modifying surface sensible and
28 latent heat fluxes, as well as atmospheric circulations (e.g., Beljaars et al., 1996; Fennessy and
29 Shukla, 1999; Viterbo and Betts, 1999; Zeng et al., 2003; Koster et al., 2004; Douville, 2010,
30 Guo et al., 2012). As indicated by Fennessy and Shukla (1999), the strength of the impact of
31 the initial soil wetness differences was dependent on several factors, such as the areal extent
32 and magnitude of the initial soil wetness difference and the persistence of the soil wetness
33 difference. In this context, the impact of the initial soil wetness difference on numerical

1 modelling, using a coupled model, also depends on the simulation lengths or the time scales
2 of interest.

3 Therefore, regarding short-range high-temperature weather or heat wave simulations, the
4 following questions arise: (1) Are short-range (e.g., 24-hour) simulations sensitive to the
5 change in soil moisture and, if so, to what extent? (2) What is the mechanism responsible for
6 the change in simulated variables (e.g., air temperature) induced by the initial soil moisture?
7 Moreover, what is the relative importance of the physical processes (e.g., surface heat transfer
8 via sensible and latent heat fluxes and atmospheric processes via advection and convection)
9 that affect the simulated temperature for continental China? The answers to these questions
10 can enhance our understanding on the influence of soil moisture and can help us to improve
11 the accuracy of high-temperature weather forecasts.

12 The objective of this paper is to quantify and explain the sensitivity of high-temperature
13 weather to initial soil moisture by answering the above questions. Hence, using different soil
14 moisture initialisations in the Noah land surface scheme in the WRF model, we perform
15 sensitivity experiments to simulate the temperature change and related quantities (e.g.,
16 sensible and latent heat fluxes, radiative fluxes, and geopotential heights) for the East China
17 high-temperature event of late July 2003. Therefore, in Sect. 2 of this paper, we describe the
18 climate background of the high-temperature event (e.g., anomalies in the 500-hPa
19 geopotential heights and surface temperatures) and the experimental design. In Sect. 3, the
20 simulation results are analysed using a comparison among the simulated surface air
21 temperature (SAT) results and observations to quantify sensitivity and further explain how
22 and to what extent the physical processes (e.g., surface heat transfer, atmospheric advection
23 and convection) affect the soil moisture-induced temperature changes. Finally, Sect. 4
24 presents a summary and conclusions of the research.

25

26 **2 Methods and data**

27 **2.1 Experimental design**

28 **2.1.1 Climate background of the simulation period**

29 Previous studies have shown that persistent, strong anomalies and an exceptionally westward
30 position of the western Pacific subtropical high were the prevalent causes of the continuous

1 high-temperature weather in southern China (mainly in southeastern continental China; see
2 area D3 in Fig. 1a) in the summer of 2003 (Lin et al., 2005; Yang and Li, 2005; Zeng et al.,
3 2011). Shown in Fig. 1b, the subtropical high in July 2003 exhibited a west-east distribution
4 that spanned 15 degrees of latitude, where the westward extent of the ridge of the 5880 gpm
5 (geopotential meters; quantitatively, 1 gpm is very close to 1 m in the troposphere) contour
6 was west of 110°E. Compared to the multi-year (1971-2000) climate, both the north-south
7 extent and area of the western Pacific subtropical high were larger for this event, the position
8 was abnormally 20 degrees west and the intensity was stronger. In the summer, East China
9 was persistently controlled by the much stronger westward ridge of the subtropical high, with
10 weaker winds and more sunny days, which result in exceptionally hot weather.

11 Figures 1c and d present the anomalies of the SAT and precipitation, respectively, that
12 occurred in July 2003 for the region; here, the climatological dataset of Willmott et al. (1998)
13 was applied. During the period, most areas south of the Yangtze River had an average SAT
14 1.5°C higher than the multiyear average, while the SAT in the Huaihe River Basin (30-36°N,
15 112-121°E) was 1°C lower than normal (Fig. 1c). In the regions to the south of the Yangtze
16 River, the precipitation was generally more than 2 mm d⁻¹ below normal, or 4 mm d⁻¹ below
17 normal for half of the area (Fig. 1d). However, there was substantially more precipitation in
18 the Yangtze River and Huaihe River basins (Fig. 1d).

19 From the distribution of day-to-day SATs (not shown), the high-temperature climate in
20 southern China, with 35°C or higher daily maximum SATs, lasted for over one month (over 2
21 months in some areas). The daily maximum SATs in July from the middle and lower reaches
22 of the Yangtze River to South China were as high as 38-40°C; the values even reached 40-
23 43°C in some areas of the south-eastern coastal region, especially in late July, which was the
24 hottest period of the summer according to 10-day moving averages of SAT over the study
25 area (Zeng et al., 2011). Record high temperatures, heat wave extents and heat wave durations
26 were set.

27 **2.1.2 WRF and the experiment schemes**

28 We investigated the sensitivity of the temperature simulations to initial soil moisture using the
29 Advanced Research WRF model (Version 3; Skamarock et al., 2008). As a community
30 mesoscale model developed by the National Center for Atmospheric Research and other
31 research institutions, WRF contains key dynamic features, such as fully compressible
32 nonhydrostatic equations, complete Coriolis and curvature terms, and includes many

1 advanced physical parameterisation schemes. The schemes adopted in this study include the
2 microphysics scheme of Lin et al. (1983), the Betts-Miller-Janjic subgrid-scale cloud scheme
3 (Janjic, 1994), the Rapid Radiation Transfer Model longwave radiation scheme (Mlawer et al.,
4 1997), the Goddard shortwave radiation scheme (Chou and Suarez, 1994), the Monin-
5 Obukhov surface layer scheme (Hong and Pan, 1996), the YSU boundary layer
6 parameterisation scheme (Hong et al., 2006), and the Noah land surface scheme (Chen and
7 Dudhia, 2001; Ek et al., 2003). Through the coupling of the land surface and atmospheric
8 boundary layer schemes, WRF accounts for land-atmosphere interactions, e.g., soil moisture-
9 air temperature feedbacks.

10 Two-way nesting is used in the simulations. The simulation domain is centred at (29°N,
11 117.5°E), with 60×70 grid points and 30-km spacing for the large domain (D1) and 127×145
12 grid points and 10-km spacing for the small domain (D2) (Fig. 1a). The vertical resolution is
13 non-uniform 31 layers with 50 hPa set as the top of the model. In late July 2003, extremely
14 high temperatures mainly occurred over the areas south of the Yangtze River in eastern China
15 (i.e., East China, denoted as area “D3” within area “D2” in Fig. 1a). Except as otherwise
16 stated, the statistical areal averages involved in the following analysis are the average values
17 of the land component of area D3.

18 Similar to Zeng et al. (2011), the hottest late July period is the focus of this paper. The initial
19 fields of the simulations are selected from 0600 UTC 20 July through 0600 UTC 29 July 2003
20 (at an interval of 24 hours), i.e., ten 24-hour integrations are performed with a suite of model
21 setups. We choose 24 hours as the integration length because initial soil moisture is relatively
22 less modified at this time scale of short-range weather. Subsequently, each integration is
23 labelled with the ending time of the experiment, e.g., “D21” represents the simulation with the
24 integration period from 0600 UTC 20 through 0600 UTC 21 July 2003.

25 To investigate the sensitivity of the short-range high-temperature weather simulation to soil
26 moisture, the initial soil moisture fields are treated as follows. First, the initial field of the
27 total volumetric soil moisture content (hereafter SMOIS) is modified at each grid point;
28 correspondingly, the values for each soil layer are modified. Second, on the basis of using the
29 analysis data to perform ten 24-hour integrations (i.e., the control run or the CTL group of
30 simulations) for late July and following Fischer et al. (2007), sensitivity experiments are
31 conducted with the modified initial soil moisture, i.e., the four groups of simulations (WET50,
32 WET25, DRY50 and DRY25) are conducted with the initial moisture content changes of

1 +50%, +25%, -50% and -25%, respectively, relative to CTL. Thus, the 24-hour simulations
2 for a specific date (e.g., the D21 simulation) have 5 initial fields of soil moisture; in total, 50
3 simulations are conducted. Meanwhile, because the SMOIS values range from 0 to 1 (the
4 value of 1 presents the land cover type of inland water), when the first-guest value of the
5 SMOIS at a grid point is larger than the saturated value in the sensitivity simulations, the
6 saturated value is set as the initial value for the integrations. Therefore, the SMOIS values for
7 the inland water remain unchanged. As an example, Fig. 2 presents the surface soil moisture
8 fields at 0600 UTC 20 July 2003 for the initial values in the D21 simulations. In Fig. 2a,
9 except for the large inland water bodies (e.g., the Yangtze River, Taihu Lake, and Poyang
10 Lake), the soil moisture contents are generally less than $0.5 \text{ m}^3 \text{ m}^{-3}$. In this case, the WET25
11 and WET50 soil moisture contents at the grid points can be increased by 25 and 50%,
12 respectively, except for few grids that approach saturation (Figs. 2d and e).

13 Once the initial and boundary conditions are defined, according to the WRF formulations,
14 both the land and atmospheric variables (e.g., atmospheric wind speeds, pressure, temperature,
15 geopotential height, soil temperature and soil moisture), as well as the surface fluxes (e.g.,
16 radiative, sensible heat and latent heat fluxes), vary over time during the model integrations;
17 these simulation results are used for the analysis.

18 It should be noted that there is no unified definition or standard of “heat wave” events. For
19 example, the National Weather Service considers the effects of temperature and relative
20 humidity, and an excessive heat warning is issued by the agency when daytime heat index
21 values are expected to reach 40.5°C or above for two consecutive days or when the values are
22 expected to exceed 46°C for any length of time (Kalkstein et al., 1996). For the Euro-
23 Mediterranean region, Stefanon et al. (2012) presented a method for defining and classifying
24 heat waves in which the events are grouped into six classes. In China, based on climate and
25 environmental characteristics, high-temperature weather is classified into three levels in the
26 context of daily maximum SAT, i.e., high temperature ($\geq 35^\circ\text{C}$), dangerously high
27 temperature ($\geq 38^\circ\text{C}$), and intensely hazardous high temperature ($\geq 40^\circ\text{C}$) (Zhang et al.,
28 2006). Because the SAT generally approaches the daily maximum value at approximately
29 1400 Beijing Time (i.e., 0600 UTC) in southeastern China (especially in summer when the
30 weather is persistently hot), following Zeng et al. (2011), we assume the SAT at 0600 UTC
31 (SAT06) is representative of the daily maximum SAT. According to observations (not shown),
32 the 35°C or higher daily maximum SAT most prominently occurred in late July 2003 over

1 southeastern China. In the context of the high-temperature classification in China, to
2 investigate the sensitivity of simulated hot weather to initial soil moisture, we therefore focus
3 on SAT06 results and related quantities for the study period of late July 2003, with an
4 integration length of 24 hours for each simulation.

5 **2.2 The data**

6 The meteorological initial and lateral boundary conditions for the WRF model, including the
7 data of the soil moisture for CTL, are derived from the National Centers for Environmental
8 Prediction (NCEP) Final (FNL) Operational Global Analysis data (1° by 1° resolution)
9 prepared operationally every six hours (00, 06, 12 and 18 UTC;
10 <http://rda.ucar.edu/datasets/ds083.2/>). The FNL analysis data are from the Global Data
11 Assimilation System that continuously collects observational data for many analyses; the data
12 are produced with the same model in the NCEP Global Forecast System (GFS), which is a
13 global spectral data assimilation and forecast model system (e.g., Whitaker et al., 2008). The
14 data are prepared approximately an hour after the GFS is initialised because such a delay
15 facilitates the use of more observational data. The GFS also uses the FNL data from the
16 previous 6-hour cycle as part of its initialisation. Moreover, the dataset is also recommended
17 for use in WRF for mesoscale weather simulations ([http://www.dtcenter.org/wrf-](http://www.dtcenter.org/wrf-nmm/users/downloads/input_data.php)
18 [nmm/users/downloads/input_data.php](http://www.dtcenter.org/wrf-nmm/users/downloads/input_data.php)).

19 To validate the temperature (i.e., SAT06) simulations, conventional observational data from
20 the meteorological stations are used. Shown in Fig. 1a, 369 stations are located in the core
21 region of East China.

22 **2.3 Analysis of physical processes**

23 We mainly focus on the change in air temperature due to the modified SMOIS. The temporal
24 change in air temperature is governed by the partial differential equation that is derived from
25 the first law of thermodynamics, i.e.,

$$26 \quad \frac{\partial T}{\partial t} = -\mathbf{V} \cdot \nabla T - w(g_d - g) + H_t, \quad (1)$$

27 where \mathbf{V} represents the horizontal wind vector, w is the vertical velocity, g_d and g are the
28 atmospheric temperature lapse rate and the dry adiabatic lapse rate, respectively, and H_t is
29 the diabatic heating term. We let

1 $T_t = \int_t \frac{\partial T}{\partial t} dt,$

2 $ADV = -\int_t \mathbf{V} \cdot \nabla T dt,$

3 $CON = -\int_t w(g_d - g) dt,$

4 and

5 $Q_t = \int_t H_t dt$

6 represent integral terms for local temperature changes, advection, convection, and diabatic
7 effects, respectively. Then, Eq. (1) can be rewritten as

8 $T_t = ADV + CON + Q_t.$ (2)

9 Thus, there are three factors (terms; units are in Kelvin) that influence T_t on the right side of
10 Eq. (2): the first term, ADV , means that warm advection causes the increase of the local
11 temperature and vice versa; the second term, CON , suggests that under stable stratification
12 ($g_d - g > 0$), ascending motion results in adiabatic cooling in the lower atmosphere and vice
13 versa, while the situation is opposite under unstable stratification ($g_d - g < 0$); and the third
14 term, Q_t , includes the diabatic influence of radiation, turbulent exchange and condensation
15 processes, among others. Except for Q_t , the other three terms of Eq. (2) can be calculated by
16 the simulation outputs; therefore, Q_t can be obtained. Thus, the relative contributions of the
17 factors to air temperature changes can also be examined.

18 Because there are few 2-m meteorological quantities in the model outputs, it is unlikely to
19 calculate directly all of the terms in Eq. (2). Therefore, we utilise the analogous relationship
20 between air temperature at 2 m and that at the lowest model level, where the model outputs
21 are adequate (see Sect. 3.2.4), to explain the extent to which the 2-m temperature is affected
22 by the physical processes.

23

1 **3 Results and discussion**

2 **3.1 Quantifying the sensitivity: preliminary results of temperature**

3 Because all the model settings and boundary and initial conditions, except the initial soil
4 moisture content, are the same in the simulations, the differences between the simulations are
5 caused by the different initial soil moisture contents. In addition, to examine the overall
6 influence of the different initial soil moisture contents on the short-range high-temperature
7 simulations for late July 2003, following Xue et al. (2001) and Zeng et al. (2011), we use the
8 ten-day means of the simulated results in the following sections to investigate the event
9 climatologically and systematically. Therefore, in this section, we preliminarily analyse the
10 soil moisture-induced differences in the ten-day mean SAT06 values of the simulations.

11 **3.1.1 Spatial distribution**

12 As discussed above, the spatial SAT06 distributions are approximately the maximum SAT
13 values over East China and the occurrence of the hottest weather during the study period.
14 Figure 3 provides the average distributions of the ten-day mean SAT06 for the simulations.
15 The central position, range and strength of the high temperature simulated in the CTL run (Fig.
16 3b) are basically consistent with those in the NCEP FNL analysis field (Fig. 3a), i.e., the areas
17 with 35°C or higher SATs are located within 26°N-32°N (the central part of the continental
18 study area). The central positioning of the high values is well simulated. Nevertheless, the
19 simulated high-temperature (above 35°C) area is slightly larger and more northward than the
20 analysis data.

21 Compared with CTL, changing the initial soil moisture can substantially change the
22 simulation results. For instance, in contrast with CTL (Fig. 3b), the central positions of the
23 high temperature of SAT06 in DRY25 (Fig. 3c) and DRY50 (Fig. 3d) remain basically
24 unchanged, but the range and intensity of the simulated high temperature are apparently
25 increased. CTL produces a simulated maximum temperature of approximately 37°C, with a
26 relatively small area that has higher values. However, the maximum DRY25 temperature is
27 higher than 38°C (i.e., dangerously high temperature), and the total area with 37°C+
28 temperatures covers most of the CTL areas above 35°C. The maximum temperature of
29 DRY50 exceeds 40°C, and the dangerously high temperature covers much of the area north of
30 26°N. Clearly, a decrease in SMOIS corresponds to an increase in the simulated SAT06.
31 Additionally, compared with CTL (Fig. 3b), the high temperature ranges and intensities in

1 WET25 (Fig. 3e) and WET50 (Fig. 3f) obviously decrease, i.e., WET25 produces a maximum
2 temperature of $\sim 36^{\circ}\text{C}$, with a relatively small area above 35°C (SAT06), and WET50 only
3 produces a maximum of $\sim 35^{\circ}\text{C}$, with a very small area above 35°C (SAT06); thus, almost no
4 high temperatures are simulated in the entire domain. In previous climate studies, regions
5 with intermediate soil moisture have been found to be sensitive to soil moisture-precipitation
6 coupling (e.g., Koster et al., 2004). Based on regional climate model simulations for the 2003
7 European heat wave, Fischer et al. (2007) suggested that the soil moisture sensitivity was low
8 in dry (near wilting point, e.g., DRY50 in their simulations) and wet (near field capacity, e.g.,
9 WET50) soil moisture conditions, and the sensitivity was high in intermediate soil moisture
10 conditions. Unlike Fischer et al. (2007), we adopt WRF for short-range weather simulations.
11 Despite the further changes in the SMOIS, the model is unable to simulate values near the
12 wilting point or field capacity for the overall study domain within 24 hours (i.e., the total soil
13 moisture does not change much at short time scales compared to long climate simulations
14 with persistent prolonged modifications to soil moisture in heat wave events; see Sect. 3.2 for
15 soil moisture variations); therefore, the SMOIS-induced sensitivity is high, at least for the
16 heat wave development in the short range. Specifically, the above results suggest that with the
17 SMOIS increase, the simulated SAT06 clearly decreases, even in some dry or wet soil
18 moisture conditions. Meanwhile, with the SMOIS change, the SAT in the lower troposphere
19 (e.g., 850 hPa) presents a change similar to the SAT06 (not shown). All of these results show
20 that the high-temperature simulations with a short-term (24-hour) integration length are very
21 sensitive to the change in initial soil moisture.

22 To assess the influence of the SMOIS change, further comparisons are made between CTL
23 and the sensitivity simulations (Figs. 3g-j). Compared with CTL, DRY25 presents a SAT06
24 increase of more than 1°C over most of the land areas (Fig. 3g), while the SAT06 in DRY50
25 rises more than 2°C (generally) and 4°C (maximally) over land (Fig. 3h). In contrast, WET25
26 reduces the temperature in most areas by more than 0.5°C (Fig. 3i), while WET50 reduces the
27 temperature by more than 1°C , with a maximum decrease greater than 2°C (Fig. 3j). For a
28 given sensitivity simulation, the amplitude of the temperature change differs in different areas;
29 these changes are closely related to the local forcings of the surface energy balance, such as
30 the sensible and latent heat fluxes (see Sect. 3.2). By comparing the four groups of sensitivity
31 simulations with CTL, it is found that the magnitude of the temperature increase in DRY50
32 (DRY25) is greater than that in WET50 (WET25); therefore, the higher sensitivity of the
33 simulated SAT06 is induced by lower soil moisture. In addition, the area with the largest

1 SAT06 change is found over/around the area with temperatures above 35°C. All of these
2 findings indicate that the change in the initial soil moisture has a very large influence on the
3 SAT06 simulation, or on the development of the short-range (24-hour) extremely high
4 temperature weather.

5 Figure 4 presents the average SAT06 values for area D3 in the simulations. In agreement with
6 the above results, the higher soil moisture simulations produce lower area-averaged SAT06
7 for each simulation (Fig. 4a). Notably, the magnitude of the SAT06 increase from DRY25
8 (25% SMOIS decrease) to DRY50 (50% SMOIS decrease) is larger than the magnitude of the
9 SAT06 decrease from WET25 (25% SMOIS increase) to WET50 (50% SMOIS increase).
10 This result is consistent with the conclusions in previous climate studies (e.g., Fischer et al.,
11 2007; Zhang and Wu, 2011), i.e., because low soil moisture strongly reduces latent cooling,
12 the surface temperature anomalies or heat waves are amplified. Our results show that during
13 the 24-hour integrations, the high temperature simulation is more sensitive to the decrease in
14 soil moisture than to the increase. The results are easily explained as follows: the lower
15 thermal inertia induced by lower soil moisture leads to higher temperatures under given
16 energy forcings. Figure 4b further presents the nonlinear changes in the ten-day mean SAT06
17 in area D3 for the five groups of simulations; the WET25-WET50, CTL-WET25, DRY25-
18 CTL and DRY50-DRY25 differences are 0.44, 0.73, 0.92 and 1.48°C, respectively. These
19 findings further confirm that high-temperature short-range weather simulations are very
20 sensitive to a decrease in the initial soil moisture.

21 3.1.2 Simulation errors

22 To examine the consistency of simulations with observations and to assess the sensitivity
23 results under different soil moisture conditions, the simulation results are interpolated to
24 meteorological stations (Fig. 1a). In the following section, the model bias (BIAS) and root-
25 mean-square error (RMSE) are applied, which are computed as

$$26 \text{BIAS} = \bar{M} - \bar{O}, \quad (3)$$

$$27 \text{RMSE} = \sqrt{\frac{1}{N} \sum_{i=1}^N (M_i - O_i)^2}, \quad (4)$$

28 where M is the simulated quantity, and O is the observation.

1 Figure 5 presents the BIAS and RMSE values for the SAT06 in each simulation. The CTL run
2 shows a SAT06 value near the observational value, with the ten-day mean SAT06 value
3 0.14°C lower than the observational value (Fig. 5a); thus, the BIAS in each sensitivity
4 simulation is generally consistent with the SAT06 difference between the simulation and CTL.
5 The ten-day mean SAT06 values of DRY50 and DRY25 are 2.5°C and 0.90°C higher,
6 respectively, than the observations, with a relative difference exceeding 150% (relative to
7 DRY25), while the SAT06 values of WET50 and WET25 are 1.5°C and 0.96°C lower,
8 respectively, with a difference as high as 50% (relative to WET25). These day-to-day results
9 further demonstrate that the high-temperature weather simulation is very sensitive to the
10 change in soil moisture and is more sensitive at a lower level of soil moisture than at a higher
11 level. In other words, hot weather can be amplified under low soil moisture conditions.
12 Similar results can be observed from the RMSE values (Fig. 5b), e.g., the average RMSE
13 values of DRY50 and DRY25 are 3.9 and 3.0°C , respectively, i.e., the difference is large.

14 **3.2 Explanation of the sensitivity: details of physical processes**

15 Regarding the mechanism responsible for the sensitivity, the SAT difference induced by
16 initial soil moisture is directly caused by different land surface energy fluxes and by modified
17 regional dynamic circulation. Among the fluxes, upward sensible heat transfer directly heats
18 the low-level atmosphere and plays a key role in influencing the SAT, while latent heat flux is
19 modified by the change in soil moisture and evaporation, which further affect the SAT. For
20 example, decreased soil moisture leads to lower evaporation and a reduced cooling effect of
21 the land surface; as a result, a higher sensible heat flux is available to heat the lower
22 troposphere.

23 **3.2.1 Soil moisture**

24 The Noah land surface scheme calculates the soil moisture for four layers with thicknesses of
25 10, 30, 60 and 100 cm for the L1, L2, L3 and L4 layers, respectively. Figure 6 shows the
26 variations of the ten-day mean soil moisture in the five groups of simulations. Overall, the
27 changes in the soil moisture within 24 hours are closely related to the depths of the soil layers
28 and the initial values of the soil moisture. The shallow soil moisture changes significantly,
29 while the deep soil moisture is less modified or nearly unchanged. Shown in Fig. 6a, the CTL
30 soil moistures of L3 and L4 change slightly, while those of L1 and L2 decrease more due to
31 continuous evaporation, which is consistent with the late July weather of sunny days and no

1 rainfall. In DRY25, the surface soil moisture appears to be recharged by the lower soil layer
2 because the surface moisture is very low (lower than that in CTL, which is normally dry), and
3 the surface soil moisture after 24 hours is still nearly unchanged (Fig. 6b). The DRY50
4 surface soil moisture is similar, but with a temporal increase (Fig. 6c). The results of WET25
5 and WET50 contrast those of the DRY simulations: the shallow soil moisture of the former
6 changes significantly due to the adequate water supply during the dry, hot weather, and the
7 model spins up with ~10% decreases in surface moisture during the first hour of the
8 integrations (Figs. 6d-e). This spin-up behaviour highlights that the initial soil moisture values
9 should be appropriately applied to specific models in response to the model configurations.

10 **3.2.2 Sensible and latent heat fluxes**

11 Previous studies showed that surface heat transfer is crucial to changes in the atmosphere (e.g.,
12 Guo et al., 2011). Figure 7 shows the ten-day mean spatial distributions of the 0600 UTC
13 sensible heat flux of the simulations. Comparing Figs. 7b-e with Figs. 3g-j, the high-value
14 area of sensible heat flux difference corresponds very well with that of the high-temperature
15 difference, and it is also consistent with the 35°C or higher temperature central area, which
16 shows that the decrease in the initial soil moisture causes the increase in sensible heat flux and
17 thus directly leads to the temperature rise. These results indicate that sensible heat flux is a
18 key factor for the simulated SAT06; this conclusion is consistent with previous studies. For
19 example, the coupling of soil moisture and temperature is mainly determined by the ability of
20 the soil moisture to affect surface fluxes (e.g., Fischer et al., 2007; Zhang et al., 2011). It also
21 shows that, similarly to long-term (e.g., three-month) climate simulations, short-range (24-
22 hour) simulations with different soil moisture values can cause changes in surface fluxes that
23 further affect and respond to simulated SAT results.

24 Corresponding to Fig. 7, Fig. 8 displays the simulated 0600 UTC latent heat fluxes. The area
25 with the small latent heat flux differences agrees with the area of the large sensible heat flux
26 differences (Figs. 8b-e vs. Figs. 7b-e) and with the high-value area of the SAT06 differences
27 (Figs. 3g-j). This result is observed because the surface latent heat flux and sensible heat flux
28 are two components that partition the surface net radiation. Given a stable forcing of net
29 radiation, the decrease in latent heat flux leads to the increase in sensible heat flux; thus, low-
30 level temperatures increase and vice versa. In addition to the land surface changes, different
31 SMOIS values that cause changes in the surface latent heat flux would also indirectly lead to

1 changes in the SAT by modifying the radiative forcing and circulation of the atmosphere
2 (addressed at the end of this subsection).

3 In addition to the above consistency of the overall spatial patterns of the SAT and fluxes, the
4 hourly variations of the ten-day mean surface quantities clearly show the high SMOIS-
5 induced sensitivities (Fig. 9) during the 24-hour periods, e.g., large flux differences appear
6 during the daytime and peak at 0400 UTC, while the SATs reach the maxima at 0600 UTC.
7 Thus, the changes in the fluxes are anterior to the SAT changes; this result is consistent with
8 many observations in the planetary boundary layer (e.g., Liu et al., 2011).

9 The daily 0600 UTC fluxes and the flux and SAT06 differences between the sensitivity
10 simulations and CTL are shown in Fig. 10. These results not only confirm the substantial
11 SMOIS-induced sensitivity in the context of single 24-hour simulations [e.g., the DRY50-
12 DRY25 sensible heat flux difference is 67 W m^{-2} larger than the WET50-WET25 difference
13 (Fig. 10a) and corresponds to an SAT06 difference of approximately 1.6°C] but also indicate
14 that features of the ten-day mean quantities at 0600 UTC are consistent with those of the ten-
15 day means averaged with hourly values. Therefore, the high-temperature differences for 0600
16 UTC may be caused by the SMOIS-induced persistent forcings during the 24 hours.

17 It is worth noting that while the SMOIS change is nonlinearly related to the change in the 24-
18 hour-averaged sensible heat flux, the change in sensible heat flux essentially corresponds to
19 the SAT06 change in an approximately linear manner (Fig. 10d).

20 As the SMOIS changes, the modified latent heat flux has more significant and complex
21 implications for the surface energy balance. Table 1 lists the ten-day mean 0600 UTC values
22 and those averaged with the hourly outputs for the surface quantities in the five groups of
23 simulations. Interestingly, the variation of the soil moisture modifies the variation of the net
24 radiation and leads to large differences between the change in sensible heat flux and the
25 change in latent heat flux, i.e., the SMOIS increase results in the larger increase in latent heat
26 flux compared with the decrease in sensible heat flux; thus, the surface net radiation increases,
27 and vice versa. For example, the CTL daily average Bowen ratio (ratio of sensible heat to
28 latent heat) is approximately 0.2; as soil moisture decreases, the Bowen ratio increases
29 according to the 24-hour means of approximately 0.3 and 0.8 in DRY25 and DRY50,
30 respectively. Owing to the increase in sensible heat flux, the SAT rises. The results of the ten-
31 day mean quantities at 0600 UTC are similar to those of the hourly values, i.e., the surface net

1 radiation increases with soil moisture and results in the increase in the sum of the sensible and
2 latent heat fluxes.

3 The results for the surface energy balance can be understood theoretically. As reported in
4 previous studies (e.g., Baldocchi et al., 2001), the Bowen ratio of well-vegetated humid areas
5 is generally less than 1; therefore, latent heat flux, other than sensible heat flux, is the primary
6 factor that partitions net radiation at the land surface. Because of the SMOIS increase, latent
7 heat flux (i.e., water vapour flux) increases much more, produces a stronger greenhouse effect
8 and strengthens the downward atmospheric longwave radiation. Further, because sunny
9 weather persisted during the simulation period, the change in the cloud-induced reflected
10 solar radiation was negligible. Therefore, the change in shortwave radiation, which is only
11 slightly modified by the SMOIS-induced water evaporation, is also suggested to be very small.
12 Hence, the SMOIS-induced pronounced change in the surface net radiative energy is largely
13 modified by the greenhouse effect of water vapour (rather than by the shortwave radiation).
14 For instance, from DRY25 to CTL, the ten-day mean net radiation based on the hourly values
15 increases by approximately 5 W m^{-2} , which is quite large (e.g., in contrast to the sensitivity of
16 the regional surface net radiation to deforestation in the Amazon Basin at a scale of 10^6 km^2 ;
17 Dickinson and Kennedy, 1992). Additionally, the 0600 UTC net radiation increases by
18 approximately 12 W m^{-2} , and the sums of the sensible and latent heat fluxes increase by
19 similar magnitudes. However, because of the SMOIS increase, the added net radiation, which
20 is induced by the increased ground heat flux, is still less than the decrease in the sums.
21 Therefore, the overall effect of the SMOIS increase is cooling at the land surface.

22 **3.2.3 Atmospheric circulation**

23 The SAT variation is closely related to the changes in the regional atmospheric circulation,
24 which is a key element of the synoptic system over the region. Regarding the atmospheric
25 circulations in the mid-level and low-level troposphere, Fig. 11 and Fig. 12 show the 500- and
26 850-hPa geopotential height fields, respectively, and the height differences caused by the
27 SMOIS change. As stated in Sect. 2, the western Pacific subtropical high is the dominant
28 control over the weather in continental China in summer; thus, a drop in the geopotential
29 height at a given pressure level corresponds to a weakening of the subtropical high
30 atmospheric circulation, and vice versa. Shown in Figs. 11 and 12, the weather during late
31 July 2003 was controlled by the subtropical high, and the SMOIS decrease leads to the
32 increase (decrease) in the 500-hPa (850-hPa) geopotential heights. For example, compared to

1 CTL, the DRY50 500-hPa geopotential height in the simulated area generally increases by
2 over 2 gpm, with a maximum increase of over 4 gpm (Fig. 11c); the soil moisture-induced
3 effect on the 850-hPa geopotential height is opposite that at 500 hPa, i.e., the SMOIS decrease
4 leads to reduced 850-hPa geopotential heights in most of the simulated areas, and vice versa.
5 Figure 13 presents the differences in the ten-day mean surface air pressure at 0600 UTC
6 between the groups of simulations. The SMOIS decrease appears to cause a decrease in the
7 surface pressure, and the area with the surface pressure reduction is consistent with the area of
8 the SAT06 increase (Figs. 13a-d vs. Figs. 3g-j). The SMOIS-induced surface pressure drop is
9 consistent with the decrease in the 850-hPa geopotential heights.

10 In previous soil moisture sensitivity experiments over North America using various climate
11 models, Oglesby and Erickson (1989) and Pal and Eltahir (2003) found heat lows at the
12 surface and enhanced positive height anomalies in the upper atmosphere because of reduced
13 soil moisture. Fischer et al. (2007) conducted sensitivity experiments for the 2003 European
14 heat wave and found a weak surface heat low and enhanced ridging in the mid-troposphere
15 due to reduced soil moisture; they suggested a positive feedback mechanism exists between
16 soil moisture, continental-scale circulation, and temperature. However, our results indicate a
17 negative soil moisture-induced feedback mechanism between atmospheric circulation and
18 temperature in the lower atmosphere in addition to positive feedback in the mid-troposphere.
19 In fact, the low-level temperature increases due to the SMOIS decrease; then, the air volume
20 expands after being heated and causes vertical and horizontal movement. Specifically, in the
21 vertical direction, the secondary "circulation", whose direction is opposite to the actual
22 airflow in the lower layer of the western Pacific subtropical high, actually results in weakened
23 low-level subsidence in the subtropical high. Along with the horizontally expanded air that
24 causes mass divergence in the lower layer, the pressure in the lower atmosphere is thus
25 reduced under the constraint of the hydrostatic balance. Meanwhile, the expanded air induced
26 by the SMOIS decrease lifts the pressure levels in the middle and upper troposphere, e.g., the
27 500-hPa geopotential height is enhanced (Fig. 11). The difference in the feedback
28 mechanisms between Fischer et al. (2007) and our study is largely explained by the dynamical
29 subtropical high, rather than a heat low, that strongly persists in the lower and upper
30 atmosphere in East China; this is similar to the sensitivity study by Zeng et al. (2011) using
31 different land surface schemes.

1 3.2.4 Physical processes: further quantitative analysis

2 As discussed in Sect. 2.3, because of the limited 2-m model output, all the terms for the
3 physical processes in Eq. (2) cannot be calculated directly. The simulation results show that
4 the variation of the air temperature ($T_{z,l}$) at the lowest model level (i.e., ~30 m above the
5 ground, where the simulation results are adequate) is basically consistent with that of the air
6 temperature at 2 m (i.e., SAT) in the simulations (e.g., shown in Fig. 14 for CTL). For
7 example, both temperatures gradually decrease with time in the afternoon, with the lowest
8 values at approximately 2100-2200 UTC. Then, the temperatures rapidly rise and are
9 maximized at approximately 0600 UTC. The consistency in the variations demonstrates that
10 in the near-surface layer, the mechanism influencing the 2-m SAT is similar to that
11 influencing $T_{z,l}$. Therefore, in this study, the advection, convection and diabatic terms in Eq.
12 (2) are computed for the lowest model level to examine the relative importance of the terms
13 for $T_{z,l}$. Similarly, an explanation of the mechanism for the SMOIS-induced SAT changes can
14 be provided.

15 Note that the strong western Pacific subtropical high was the dominant weather system during
16 the period, when mean subsidence prevailed. Specifically, the *CON* term reflects the adiabatic
17 effect of subsidence. Table 2 lists the area-averaged ten-day mean integral results of the four
18 terms in Eq. (2) for nighttime and daytime. Although the temperature advection effect (*ADV*)
19 might be relatively strong on the single-station temperature during some periods, the area-
20 averaged *ADV* values, as one of the contributors to the $T_{z,l}$ change, are so small that they can
21 be ignored in the 24-hour simulations. For the subsidence effect term, under different soil
22 moisture conditions, the *CON* values do not generally change much, especially during the
23 daytime; one exception is for the DRY cases during nighttime, which have an overall
24 warming effect as the SMOIS decreases (e.g., compared with CTL, DRY25 produces a
25 0.16°C higher value for the *CON* term). A comparison of the *CON* term during the daytime
26 with that during the nighttime indicates that the adiabatic warming effect of the mean
27 subsidence in the western Pacific subtropical high at night is much stronger than that in the
28 daytime (e.g., the DRY25-*CON* temperature rises 11.12 and 1.01°C in the nighttime and
29 daytime, respectively); thus, the regional atmospheric circulation may have a much more
30 significant influence on the temperature change in the surface layer at night. The difference in
31 the heating effect is mainly due to the stratification difference between day and night in the
32 subtropical high, i.e., the daytime boundary layer is relatively well mixed compared to the

1 nighttime boundary layer, and mean subsidence has a greater heating influence on the
2 hydrostatically stable lower atmosphere during the nighttime than during the daytime. In
3 addition, because the nighttime subsidence effect is more affected by the SMOIS change than
4 the nearly unchanged daytime subsidence effect, relative to the WET conditions, an enhanced
5 temperature increase is induced under the DRY conditions at the end of the 24-hour
6 integrations (Table 2).

7 Compared with the absolute CON values for nighttime and daytime, the corresponding
8 absolute Q_t values are larger, i.e., the absolute CON values are approximately two thirds of
9 the magnitude of the absolute Q_t values at night and less than one fourth of the absolute Q_t
10 values in the daytime (Table 2). This finding indicates the dominant role of diabatic processes
11 over the role of subsidence at the intra-daily time scales. During the nighttime, with the
12 occurrence of the boundary-layer temperature inversion induced by the longwave radiative
13 cooling at the land surface, the turbulence-induced diabatic cooling effect is larger than the
14 adiabatic temperature increase effect; therefore, the surface air becomes colder. During the
15 daytime, along with the modified stratifications, diabatic heating dominates and is much
16 stronger than the subsidence-induced adiabatic temperature increase, which is much weaker
17 compared to the nighttime. Interestingly, although the diabatic effect dominates the
18 subsidence effect during the nighttime and daytime [e.g., the nighttime value is -15.33°C
19 (11.01°C) and the daytime value is 4.21°C (0.99°C) for the WET25 Q_t (CON) term], because
20 the Q_t term has opposite signs during the various time periods, the overall diabatic effect does
21 not dominate the subsidence effect for the 24-hour simulations. The diabatic effect is stronger
22 than the subsidence effect in the CTL and WET (DRY) cases over the 24 hours, and vice
23 versa. For instance, WET25 (DRY25) produces the values of 12.05°C and -12.76°C (12.20°C
24 and -11.37°C) for the 24-hour CON and Q_t terms, respectively. Contrary to the CON
25 consistent heating effect, the Q_t term has an overall cooling effect. However, it should be
26 noted that the overall temperature rise, in response to the SMOIS decrease (e.g., the increase
27 in the 24-hour T_t term compared to CTL), is mainly caused by the decreased cooling effect of
28 the Q_t term instead of the increased heating effect of the CON term, e.g., for the 24-hour
29 integrations, the T_t term changes from -0.14°C (CTL) to 0.83°C (DRY25), and the change is
30 accompanied by a difference in the CON term (from 12.04 to 12.20°C) and a much larger
31 difference in the Q_t term (from -12.18 to -11.37°C). These results demonstrate that the

1 overall diabatic processes are affected much more strongly by the SMOIS change. A closer
2 comparison shows that this sensitivity is higher under the DRY conditions (Table 2), as is
3 consistent with the sensitivity findings for SAT06 in Sect. 3.

4 In the 12-day simulations of warm-season convection, Trier et al. (2008) suggested that the
5 initial soil moisture had an important influence on thermodynamic variables, particularly
6 when the ground heating is the strongest in the daytime and the subsequent period. Our results
7 confirm this issue and also show that the SMOIS-induced change in the nighttime cooling can
8 exceed half of the change in the daytime heating in the high-temperature simulations (e.g.,
9 from CTL to DRY25, the Q_e term decreases by 0.30°C during the nighttime and increases by
10 0.57°C during the daytime; Table 2).

11 Similarly, subsidence and diabatic processes play important roles in modifying the 2-m air
12 temperature (SAT) change, in which the diabatic processes dominate the adiabatic subsidence
13 during the daytime and nighttime in the subtropical high. Additionally, the diabatic effect on
14 the SAT variation is affected more strongly by the soil moisture change, e.g., with the SMOIS
15 decrease, the SAT tends to increase, mainly because of the decreased cooling effect of the
16 diabatic processes in the 24-hour integrations. Because of the dry climate background in East
17 China in late July 2003, sensible heat flux played a dominant role in modifying the SAT
18 among the low-level diabatic processes, such as sensible and latent heating and radiation
19 processes. Therefore, primarily through modifying the surface sensible heat flux, the initial
20 soil moisture affects the simulation of extremely high temperatures in late July 2003 in East
21 China.

22 Notably, when only CTL is taken into account, during late July, the diabatic processes are
23 slightly more important than mean subsidence over the region (i.e., the sign of the SAT
24 change is opposite of the subsidence term during the 24-hour periods in CTL; Table 2). This
25 shows the relative importance of physical processes in the hottest phase. For periods with
26 lower temperatures, the values of both the diabatic and subsidence terms are reduced. Given
27 invariant signs for both, it is unlikely to pinpoint which term would dominate using a
28 theoretical analysis only; thus, follow-up numerical studies are needed for other cases.

29

1 **4 Summary and conclusions**

2 This paper quantifies and explains the sensitivity of WRF-simulated high-temperature
3 weather to various initial soil moisture (SMOIS) conditions in a 24-hour period. Five groups
4 of simulations are conducted in the East China for an extreme high-temperature event in late
5 July 2003.

6 We focus on SAT06, which is approximately the daily maximum temperature in East China.
7 The ten-day mean results indicate that CTL can generally reproduce the high-temperature
8 event. However, the simulated event is also sensitive to the SMOIS changes. When the
9 SMOIS is decreased, the central position of the high SAT06 values does not change much,
10 while the maximum SAT06 change mainly occurs over the areas with temperatures above
11 35°C, which is accompanied by the temperature increase and the enlarged areas with the high
12 temperatures. Compared with CTL, DRY25 (DRY50) results in a 1°C (2°C) SAT06 increase,
13 in general, over land in East China; the low soil moisture amplifies the high temperatures in
14 the simulations.

15 The modified SMOIS changes the surface fluxes and atmospheric circulation, which play
16 different roles in modifying the SAT06. Sensible heat fluxes directly heat the lower
17 atmosphere and present difference fields that are consistent with those of SAT06. Therefore,
18 the SMOIS-induced sensible heat flux change could be the most significant factor in the
19 SAT06 change. Low soil moisture can reduce evaporation such that the land surface
20 temperature increases more easily; therefore, downward longwave radiation and sensible heat
21 flux can increase, and the lower atmosphere is likely to be heated. The SMOIS increase is
22 found to modify the partitioning between sensible and latent heat fluxes. Specifically, the
23 increased magnitude of latent heat flux is larger than the decreased magnitude of sensible heat
24 flux. With the increase in the latent heat (evaporation), the greenhouse effect induced by
25 water vapour is reinforced. The result is an enhanced surface net radiation, e.g., from DRY25
26 to CTL, the net radiation increases by 5 W m⁻².

27 Overall, a SMOIS-induced negative feedback exists in the lower layer between the low-level
28 temperature and the circulation, while positive feedback exists in the mid-troposphere, e.g.,
29 the low-level SAT increases due to the SMOIS decrease, the geopotential heights lower and
30 the subtropical high in the lower atmosphere weakens, and vice versa.

31 Finally, we adopt an analogous relationship between the air temperature at the lowest model
32 level and the 2-m air temperature (SAT) to explain how the initial soil moisture influences the

1 simulated SAT via different processes. The results suggest that the diabatic processes
2 dominate the adiabatic subsidence regarding the SAT changes in the WET and CTL
3 simulations; the diabatic processes are affected more strongly by the SMOIS changes in all
4 the simulations. Although the diabatic processes have opposite effects during different time
5 periods (i.e., heating and cooling during the daytime and nighttime, respectively), they have
6 an overall cooling effect on the SAT in the 24-hour simulations. Interestingly, although the
7 diabatic processes dominate over subsidence during the daytime and nighttime, they are not
8 necessarily dominant during the 24-hour periods.

9 Additionally, we should note that this sensitivity study is implemented using a regional
10 weather model whose performance is affected by initial and boundary conditions and model
11 setups. For follow-up studies, using more cases and adopting more suites of model settings to
12 explore soil moisture effects would help us better understand the issue of soil-moisture-
13 induced sensitivity of high-temperature/heat-wave events.

14

15 **Acknowledgements**

16 The authors would like to thank Dr. W Lu and two anonymous reviewers for their helpful
17 comments on the manuscript. This work was supported by the National Natural Science
18 Foundation of China (Grant Nos. 41275012 and 41205073).

1 **References**

- 2 Baldocchi, D., Falge, E., Gu, L., Olson, R., Hollinger, D., Running, S., Anthoni, P., Bernhofer,
3 C., Davis, K., Evans, R., Fuentes, J., Goldstein, A., Katul, G., Law, B., Lee, X., Malhi, Y.,
4 Meyers, T., Munger, W., Oechel, W., Paw U, K. T., Pilegaard, K., Schmid, H. P., Valentini,
5 R., Verma, S., Vesala, T., Wilson, K., and Wofsy, S.: FLUXNET: A new tool to study the
6 temporal and spatial variability of ecosystem-scale carbon dioxide, water vapor, and energy
7 flux densities, *B. Am. Meteorol. Soc.*, 82, 2415–2434, 2001.
- 8 Barriopedro, D., Fischer, E. M., Luterbacher J., Trigo, R. M., and Garcia-Herrera, R.: The
9 hot summer of 2010: Redrawing the temperature record map of Europe, *Science*, 332,
10 doi:10.1126/science.1201224, 2011.
- 11 Beljaars, A. C. M., Viterbo, P., Miller, M. J., and Betts, A. K.: The anomalous rainfall over
12 the United States during July 1993: Sensitivity to land surface parameterization and soil
13 moisture, *Mon. Weather Rev.*, 124, 362–383, 1996.
- 14 Chen, F., and Dudhia, J.: Coupling an advanced land-surface hydrology model with the Penn
15 State-NCAR MM5 modeling system. Part I: Model description and implementation, *Mon.*
16 *Weather. Rev.*, 129, 569–585, 2001.
- 17 Chou, M. D., and Suarez, M. J.: An efficient thermal infrared radiation parameterization for
18 use in general circulation models, *NASA Tech. Memo.*, 104606, 3, 85 pp., 1994.
- 19 Dickinson, R. E., and Kennedy, P.: Impacts on regional climate of Amazon deforestation,
20 *Geophys. Res. Lett.*, 19, 1947–1950, 1992.
- 21 Donat, M. G., Alexander, L. V., Yang, H., Durre, I., Vose, R., and Caesar, J. : Global land-
22 based datasets for monitoring climatic extreme, *B. Am. Meteorol. Soc.*, 94, 997–1006, 2013.
- 23 Douville, H.: Relative contribution of soil moisture and snow mass to seasonal climate
24 predictability: A pilot study, *Clim. Dynam.*, 34, 797–818, 2010.
- 25 Ek, M. B., Mitchell, K. E., Lin Y., Rogers, E., Grunmann, P., Koren, V., Gayno, G., and
26 Tarpley, J. D.: Implementation of Noah land surface model advances in the National Centers
27 for Environmental Prediction operational Mesoscale Eta Model, *J. Geophys. Res.*, 108, 8851,
28 doi:10.1029/ 2002JD003296, 2003.
- 29 Fennessy, M. J., and Shukla, J.: Impact of initial soil wetness on seasonal atmospheric
30 prediction, *J. Climate*, 12, 3167–3180, 1999.

1 Fennessy, M. J., and Kinter, J. L.: Climatic Feedbacks during the 2003 European heat wave, *J.*
2 *Climate*, 24, 5953-5967, 2011.

3 Ferranti, L., and Viterbo, P.: The European summer of 2003: Sensitivity to soil water initial
4 conditions, *J. Climate*, 19, 3659-3680, 2006.

5 Fischer, E. M., Seneviratne, S. I., Vidale, P. L., Lüthi, D., and Schär, C.: Soil moisture–
6 atmosphere interactions during the 2003 European summer heat wave, *J. Climate*, 20, 5081–
7 5099, 2007.

8 Guo, Z., Dirmeyer, P. A., and DelSole, T.: Land surface impacts on subseasonal and seasonal
9 predictability, *Geophys. Res. Lett.*, 38, L24812, doi:10.1029/2011GL049945, 2011.

10 Guo, Z., Dirmeyer, P. A., DelSole, T., and Koster, R. D.: Rebound in atmospheric
11 predictability and the role of the land surface, *J. Climate*, 25, 4744–4749, 2012.

12 Hirschi, M., Seneviratne, S. I., Alexandrov, V., Boberg, F., Boroneant, C., Christensen, O. B.,
13 Formayer, H., Orłowsky, B., and Stepanek, P.: Observational evidence for soil-moisture
14 impact on hot extremes in southeastern Europe, *Nat. Geosci.*, 4, 17–21, 2011.

15 Holt, T., Niyogi, D., Chen, F., LeMone, M. A., Manning, K., and Qureshi, A. L.: Effect of
16 Land- Atmosphere Interactions on the IHOP 24–25 May 2002 Convection Case, *Mon.*
17 *Weather Rev.*, 134, 113–133, 2006.

18 Hong, S-Y., and Pan, H-L.: Nonlocal boundary layer vertical diffusion in a medium-range
19 forecast model, *Mon. Weather Rev.*, 124, 2322–2339, 1996.

20 Hong, S.-Y., Noh, Y., and Dudhia, J.: A new vertical diffusion package with an explicit
21 treatment of entrainment processes, *Mon. Weather Rev.*, 134, 2318–2341,
22 doi:10.1175/MWR3199.1, 2006.

23 Janjic, Z. I.: The step-mountain Eta coordinate model: Further developments of the
24 convection, viscous sub-layer and turbulence closure schemes, *Mon. Weather Rev.*, 122, 927–
25 945, 1994.

26 Kalkstein, L. S., Jamason, P. F., Greene, J. S., Libby, J., and Robinson, L.: The Philadelphia
27 hot weather-health watch/warning system: Development and application, summer 1995, *B.*
28 *Am. Meteorol. Soc.*, 77, 1519–1528, 1996.

29 Koster, R. D., Dirmeyer, P. A., Guo, Z., Bonan, G., Chan, E., Cox, P., Gordon, C. T., Kanae,
30 S., Kowalczyk, E., Lawrence, D., Liu, P., Lu, C. H., Malyshev, S., McAvaney, B., Mitchell,

1 K., Mocko, D., Oki, T., Oleson, K., Pitman, A., Sud, Y. C., Taylor, C. M., Verseghy, D.,
2 Vasic, R., Xue, Y., and Yamada, T.: Regions of strong coupling between soil moisture and
3 precipitation, *Science*, 305, 1138–1141, 2004.

4 Koster, R. D., Sud, Y. C., Guo, Z., Dirmeyer, P. A., Bonan, G., Oleson, K. W., Chan, E.,
5 Verseghy, D., Cox, P., Davies, H., Kowalczyk, E., Gordon, C. T., Kanae, S., Lawrence, D.,
6 Liu, P., Mocko, D., Lu, C.-H., Mitchell, K., Malyshev, S., McAvaney, B., Oki, T., Yamada,
7 T., Pitman, A., Taylor, C. M., Vasic, R., and Xue, Y.: GLACE: The Global Land–
8 Atmosphere Coupling Experiment. Part I: Overview, *J. Hydrometeor.*, 7, 590–610, 2006.

9 Larsen, J.: Record heat wave in Europe takes 35,000 lives. Earth Policy Institute, p. 1, 2003.

10 Lau, W. K. M., and Kim, K.-M.: The 2010 Pakistan flood and Russian heat wave:
11 Teleconnection of hydrometeorological extremes, *J. Hydrometeor.*, 13, 392–403, 2012.

12 Lei, M., Niyogi, D., Kishtawal, C., Pielke Sr., R. A., Beltrán-Przekurat, A., Nobis, T. E., and
13 Vaidya, S. S.: Effect of explicit urban land surface representation on the simulation of the 26
14 July 2005 heavy rain event over Mumbai, India, *Atmos. Chem. Phys.*, 8, 5975-5995,
15 doi:10.5194/acp-8-5975-2008, 2008.s

16 Lin, J., Bi, B. G., and He, J. H.: Physical mechanism responsible for western Pacific
17 subtropical high variation and hot wave in southern China in July 2003, *Chinese J. Atmos.*
18 *Sci.*, 29, 594-599, 2005 (in Chinese).

19 Lin, Y.-L., Farley, R. D., and Orville, H. D.: Bulk parameterization of the snow field in a
20 cloud model, *J. Clim. Appl. Meteorol.*, 22, 1065–1092, 1983.

21 Liu, H., Blanken, P. D., Weidinger, T., Nordbo, A., and Vesala, T.: Variability in cold front
22 activities modulating cool-season evaporation from a southern inland water in the USA,
23 *Environ. Res. Lett.*, 6, 024022, 2011.

24 Lyon, B., and Dole, R. M.: A diagnostic comparison of the 1980 and 1988 U.S. summer heat
25 wave-droughts, *J. Climate*, 8, 1658–1675, 1995.

26 Mlawer, E. J., Taubman, S. J., Brown, P. D., Iacono, M. J., and Clough, S. A.: Radiative
27 transfer for inhomogeneous atmosphere: RRTM, a validated correlated-k model for the long-
28 wave, *J. Geophys. Res.*, 102(D14), 16663–16682, doi:10.1029/97JD00237, 1997.

29 Oglesby, R. J. and Erickson, D.: Soil moisture and the persistence of North American drought,
30 *J. Climate*, 2, 1362–1380, 1989.

- 1 Pal, J. S., and Eltahir, E. A. B.: A feedback mechanism between soil moisture distribution and
2 storm tracks, *Q. J. Roy. Meteor. Soc.*, 129, 2279–2297, 2003.
- 3 Pielke, R. A.: Influence of the spatial distribution of vegetation and soils on the prediction of
4 cumulus convective rainfall, *Rev. Geophys.*, 39, 151-177, 2001.
- 5 Seneviratne, S.I., Koster, R.D., Guo, Z., Dirmeyer, P. A., Kowalczyk, E., Lawrence, D., Liu,
6 P., Lu, C.-H., Mocko, D., Oleson, K.W., and Verseghy, D.: Soil moisture memory in AGCM
7 simulations: Analysis of Global Land-Atmosphere Coupling Experiment (GLACE) data, *J.*
8 *Hydrometeor.*, 7, 1090-1112, 2006.
- 9 Shukla J., and Mintz, Y.: Influence of the land-surface evapotranspiration on the Earth's
10 climate, *Science*, 215, 1498-1500, 1982.
- 11 Skamarock, W. C., Klemp, J., Dudhia, J., Gill, D. O., Barker, D. M., Duda, M. G., Huang, X.
12 Y., Wang, W., and Powers, J. G.: A Description of the Advanced Research WRF Version 3,
13 NCAR Technical note NCARTN-475+STR, Natl. Cent. for Atmos. Res., Boulder, CO, USA,
14 113 pp., 2008.
- 15 Stefanon, M., D'Andrea, F., and Drobinski, P. : Heatwave classification over Europe and the
16 Mediterranean region, *Environ. Res. Lett.* 7, 014023, 2012.
- 17 Sun, J., Trier, S. B., Xiao, Q., Weisman, M. L., Wang, H., Ying, Z., Xu, M., and Zhang, Y.:
18 Sensitivity of 0–12-h warm-season precipitation forecasts over the central United States to
19 model initialization, *Weather Forecast.*, 27, 832–855, 2012.
- 20 Tan, J., Zheng, Y., and Song, G.: Heat wave impacts on mortality in Shanghai, 1998 and 2003,
21 *Int. J. Biometeorol.*, 51, 193-200, 2007.
- 22 Trier, S. B., Chen, F., and Manning K. W.: Sensitivity of the PBL and precipitation in 12-day
23 simulations of warm-season convection using different land surface model and soil wetness
24 conditions, *Mon. Weather Rev.*, 136, 2321-2343, 2008.
- 25 Viterbo, P., and Betts, A. K.: Impact of the ECMWF reanalysis soil water on forecasts of the
26 July 1993 Mississippi flood, *J. Geophys. Res.*, 19, 361–366, 1999.
- 27 Vinnikov, K. Y., and Yeserkepova, I. B.: Soil moisture: Empirical data and model results, *J.*
28 *Climate*, 4, 66–79, 1990.
- 29 Whitaker, J. S., Hamill, T. M., Wei, X., Song, Y., and Toth, Z.: Ensemble data assimilation
30 with the NCEP Global Forecast System, *Mon. Weather Rev.*, 136, 463–482, 2008.

1 Willmott, C. J., Matsuura, K., and Legates, D. L.: Global air temperature and precipitation:
2 RegridDED monthly and annual climatologies (Version 2.01), available at:
3 <http://climate.geog.udel.edu/> (last access: 6 May 2014), 2013.

4 Wolfson, N., Atlas, R., and Sud, Y. C.: Numerical experiments related to the summer 1980
5 U.S. heat wave, *Mon. Weather Rev.*, 115, 1345–1357, 1987.

6 World Meteorological Organization: The Global Climate 2001-2010: A decade of climate
7 extremes - Summary Report. WMO-No. 1119, 2013.

8 Xue, Y., Zeng, F. J., Mitchell, K. E., Janjic, Z., and Rogers, E.: The impact of land surface
9 processes on simulations of the U.S. hydrological cycle: A case study of the 1993 flood using
10 the SSiB land surface model in the NCEP Eta regional model, *Mon. Weather Rev.*, 129,
11 2833–2860, 2001.

12 Yang, H., and Li, C. Y.: Diagnostic study of serious high temperature over South China in
13 2003 summer, *Climatic and Environmental Research*, 10, 81-85, 2005 (in Chinese).

14 Zeng, X.-M., Zhao, M., Su, B., Tang, J., Zheng, Y., Zhang, Y., and Chen, J.: Effects of the
15 land-surface heterogeneities in temperature and moisture from the “combined approach” on
16 regional climate: A sensitivity study, *Global Planet. Change* 37, 247–263, 2003.

17 Zeng, Song, S., Zheng, Y., and Liu, H.: Sensitivity of simulated Wu, Z., Xiong, S., X.-M.,
18 short-range high-temperature weather to land surface schemes by WRF, *Science China: Earth*
19 *Sciences*, 54, 581-590, DOI:10.1007/s11430-011-4181-6, 2011.

20 Zhang, J., and Wu, L.: Land-atmosphere coupling amplifies hot extremes over China, *Chinese*
21 *Sci. Bull.*, 56, 581–590, doi:10.1007/s11434-011-4628-3, 2011.

22 Zhang, S., Zhang, D., Wang, S., and Song, Y.: Climatic characteristics of summer high
23 temperature and assessment methods in the large cities of North China, *J. Geogr. Sci.*, 16, 13-
24 22, 2006.

25
26
27
28
29

1
2
3
4
5
6
7
8
9
10
11
12
13
14
15
16
17
18
19
20
21
22

Tables

Table 1. Ten-day means of 24-hour-averaged and 0600-UTC sensible heat flux (SHF; $W m^{-2}$), latent heat flux (LHF; $W m^{-2}$), LHF plus SHF, net radiation (RN; $W m^{-2}$), and surface air temperatures (SAT; $^{\circ}C$) for the five groups of simulations.

	SHF		LHF		SHF+LHF		RN		SAT	
	24 h	06 UTC	24 h	06 UTC	24 h	06 UTC	24 h	06 UTC	24 h	06 UTC
DRY50	75.1	241.5	92.5	234.4	167.6	475.9	210.7	623.4	31.34	36.19
DRY25	45.8	159.2	133.3	340.4	179.1	499.7	220.8	646.9	30.68	34.75
CTL	31.4	119.3	154.7	393.8	186.1	513.1	226.0	658.7	30.21	33.79
WET25	21.3	91.7	170.8	432.1	192.1	523.8	230.1	666.8	29.81	33.06
WET50	15.8	76.8	180.1	452.3	195.9	529.1	232.2	670.3	29.57	32.62

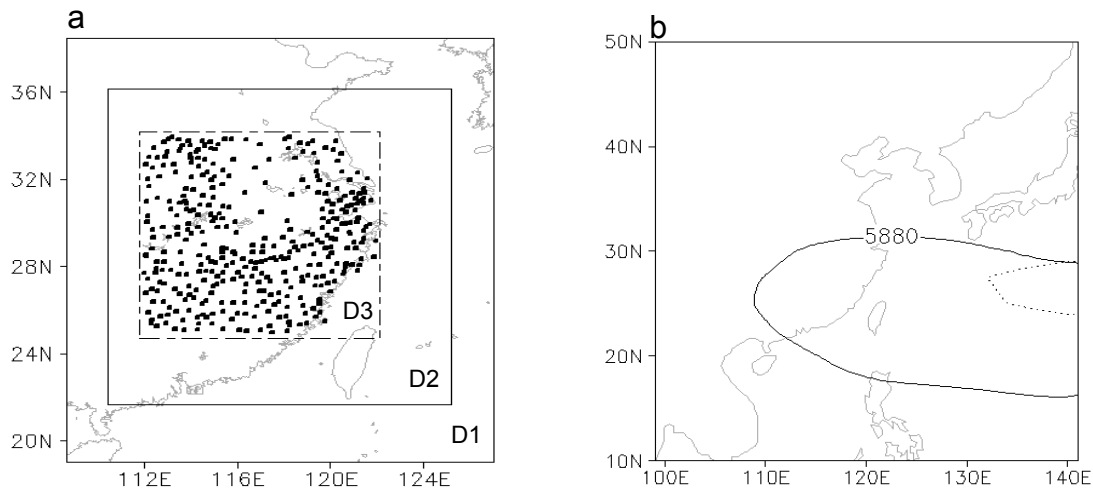
1
2
3
4
5
6
7

Table 2. Area-averaged ten-day mean integral results of the four terms in the $T_{z,t}$ equation [i.e., Eq. (2)] for 24 hours, nighttime (1100-2200 UTC) and daytime (2200-0600 UTC) (unit: °C). Note that the daytime is divided into two periods (by the night hours) in the 24-hour integrations, and only one part, which is assumed to be reasonable and have little influence on the analysis, is considered in the statistics.

	T_t			ADV			CON			Q_t		
	24 h	Nighttime	Daytime	24 h	Nighttime	Daytime	24 h	Nighttime	Daytime	24 h	Nighttime	Daytime
DRY50	2.22	-5.12	7.37	-2.6E-05	-1.2E-05	4.4E-05	12.60	11.42	1.01	-10.38	-16.54	6.34
DRY25	0.83	-4.70	6.24	6.2E-05	2.8E-05	1.6E-05	12.20	11.12	1.01	-11.37	-15.72	5.24
CTL	-0.14	-4.51	5.66	-1.8E-05	-4.9E-06	2.7E-06	12.04	10.91	0.98	-12.18	-15.42	4.67
WET25	-0.71	-4.32	5.20	-1.8E-04	3.0E-05	-2.1E-04	12.05	11.01	0.99	-12.76	-15.33	4.21
WET50	-1.20	-4.24	4.92	1.0E-04	1.2E-04	-3.0E-05	12.01	11.06	0.98	-13.21	-15.30	3.94

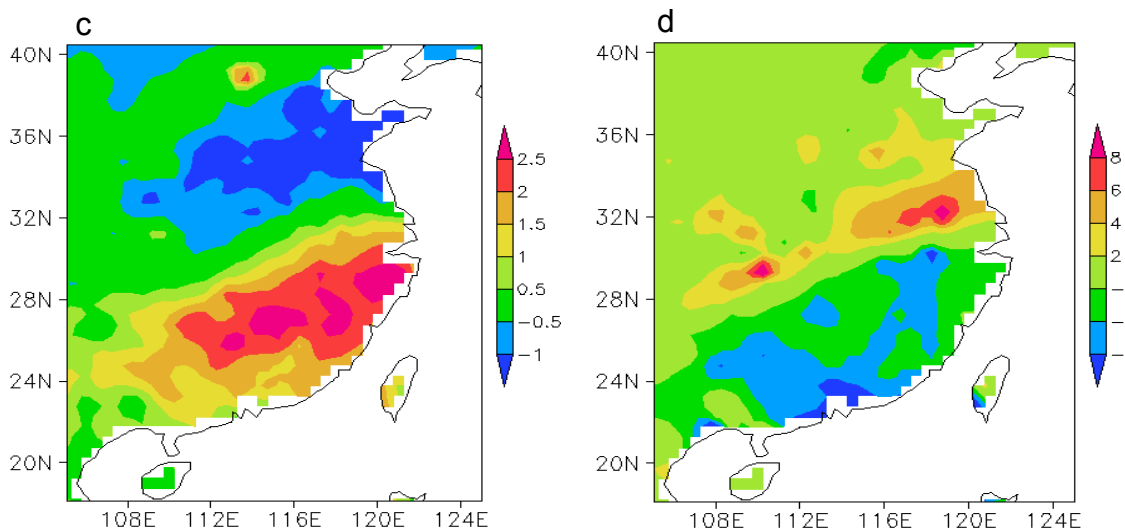
1 **Figures (please refer to the PDFs for better presentations)**

2



3

4



5

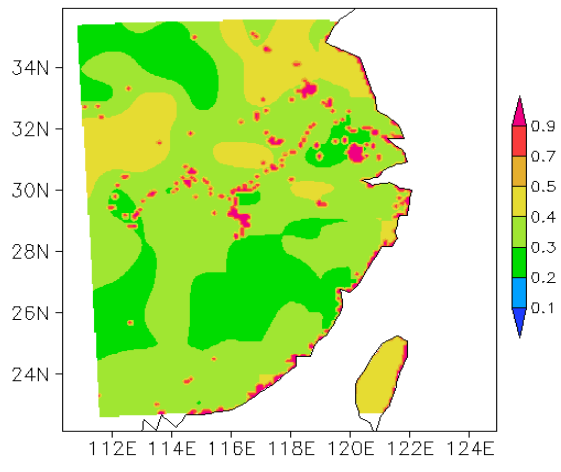
6

7 **Fig. 1.** The study areas and climatology. (a) The model domain, where the D1 and D2 sub-
8 areas are the large and nested areas, respectively, while D3 is the “core” region of
9 southeastern China, where the extremely high temperatures occurred (the meteorological
10 stations are marked by dots). (b) The 500-hPa 5880-gpm contours of the climatological
11 averages for July 2003 (solid line) and the base period (1971-2000; dashed line). (c) The July
12 2003 SAT anomaly, i.e., departures from the base-period (1971-2000) average (unit: °C). (d)
13 Same as (c) but for precipitation (units: mm d⁻¹).

14

1

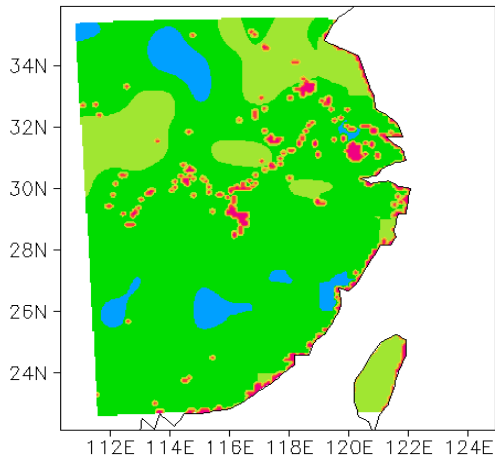
a CTL



2

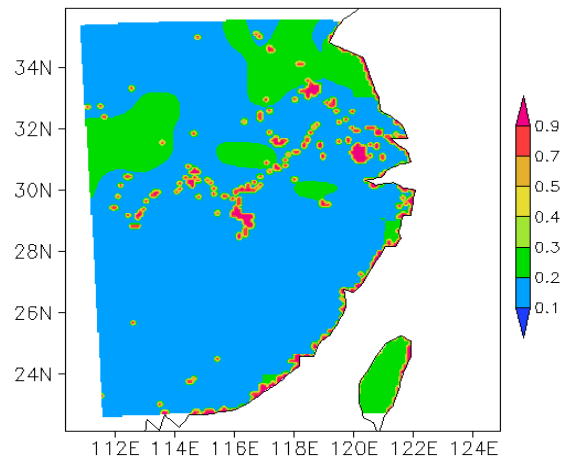
3

b DRY25



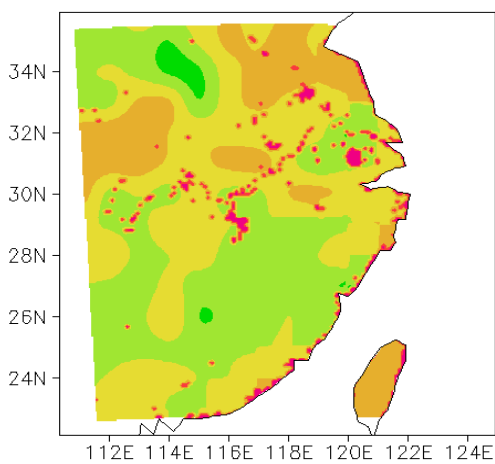
4

c DRY50



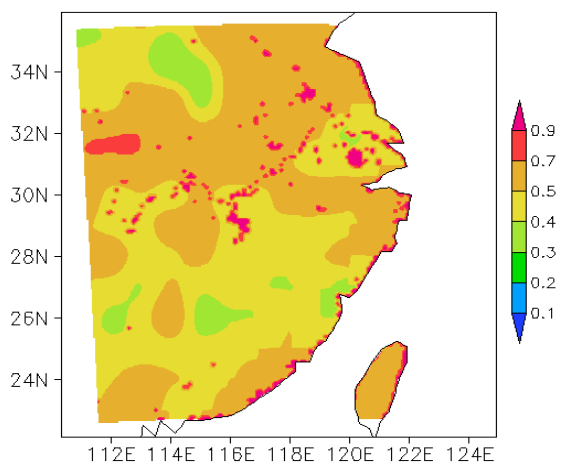
5

d WET25



6

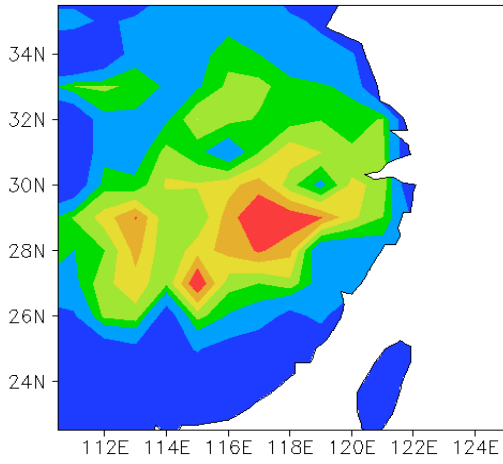
e WET50



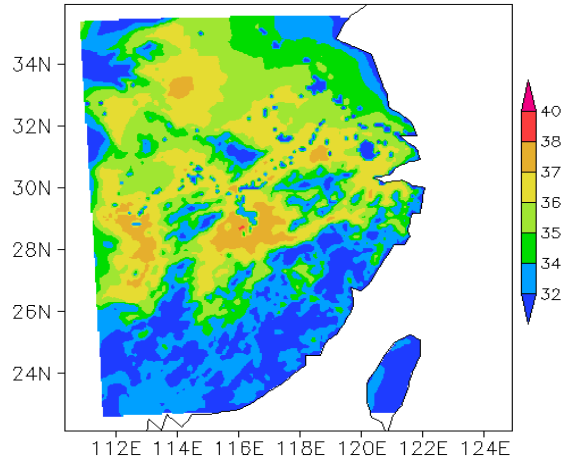
7 **Fig. 2.** The initial surface soil moisture fields at 0600 UTC 20 July 2003 in the D21
 8 simulations (units: $\text{m}^3 \text{m}^{-3}$).

1

a NCEP



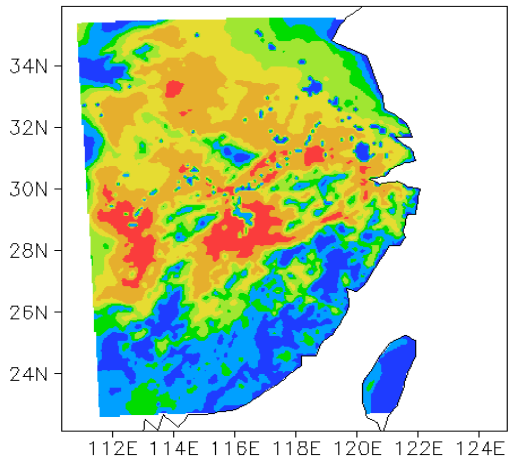
b CTL



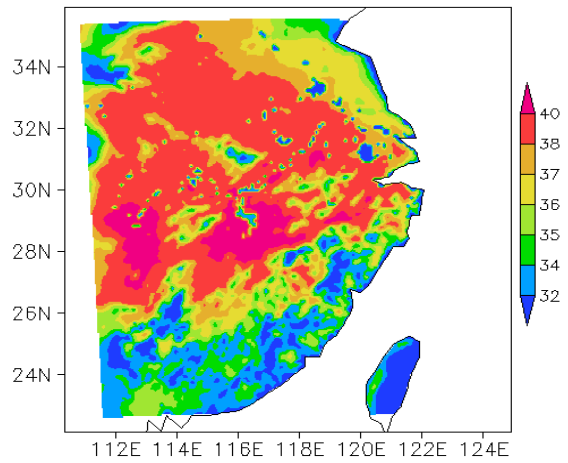
2

3

c DRY25



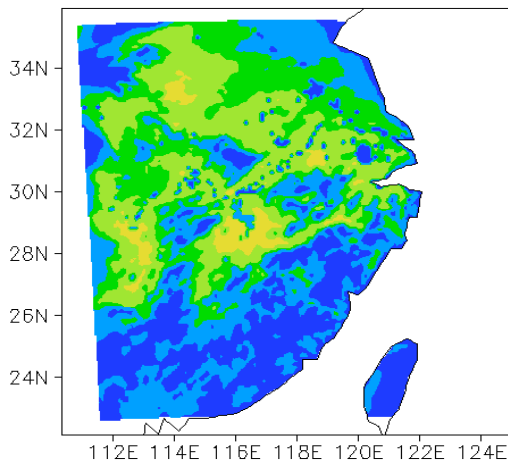
d DRY50



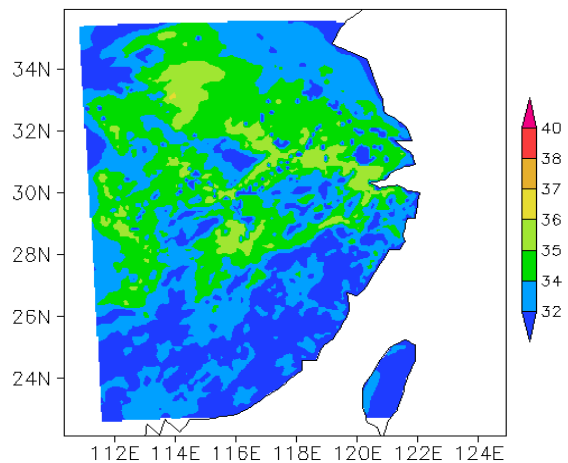
4

5

e WET25



f WET50



6

7 **Fig. 3.** (To be continued).

8

1
2
3
4
5
6
7
8
9
10
11
12
13
14

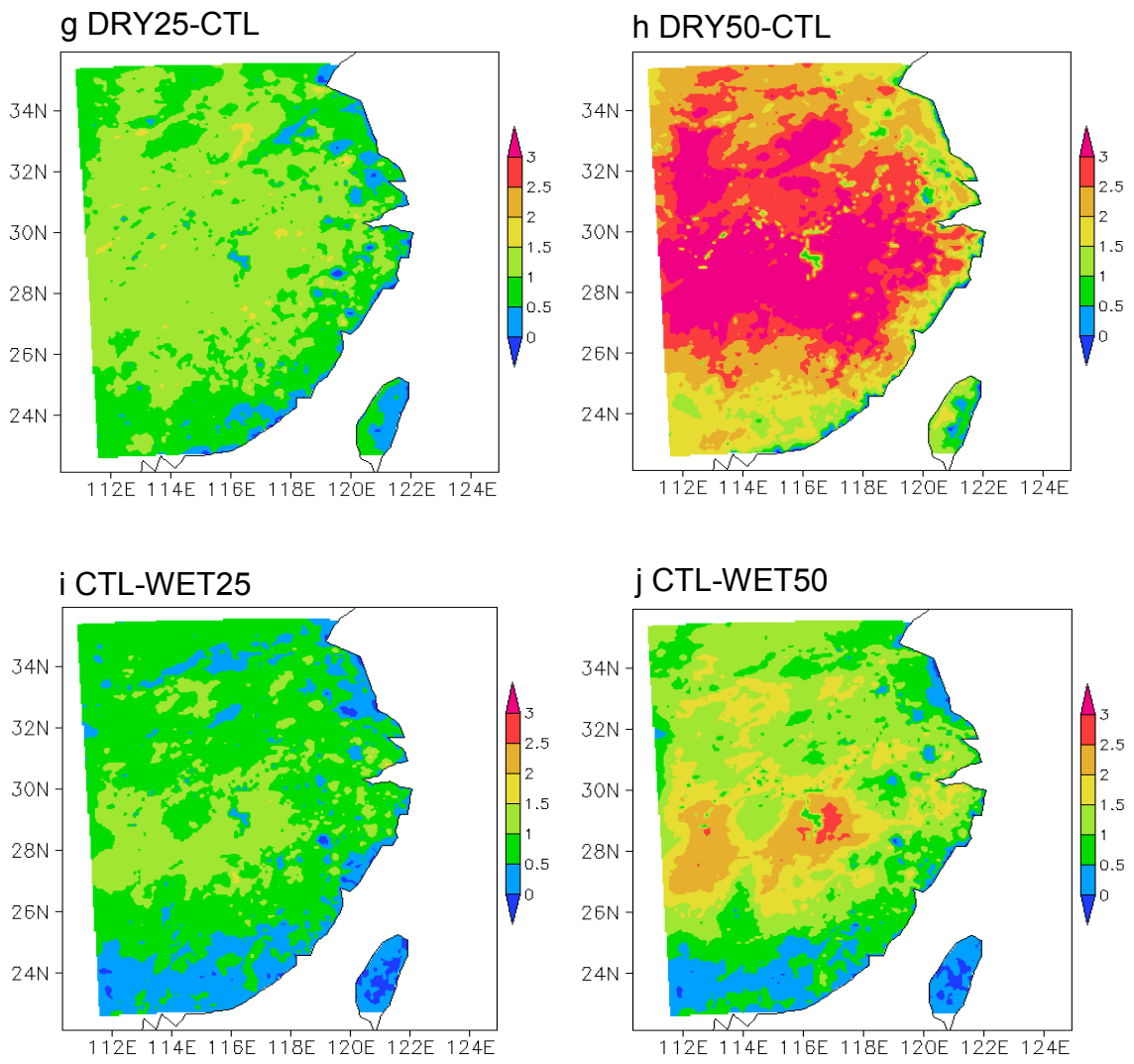


Fig. 3. The spatial distributions of the ten-day mean SAT06 in the simulations (unit: °C).

1
2
3
4
5
6
7
8
9
10
11
12
13
14
15
16
17
18
19
20
21
22
23
24
25
26

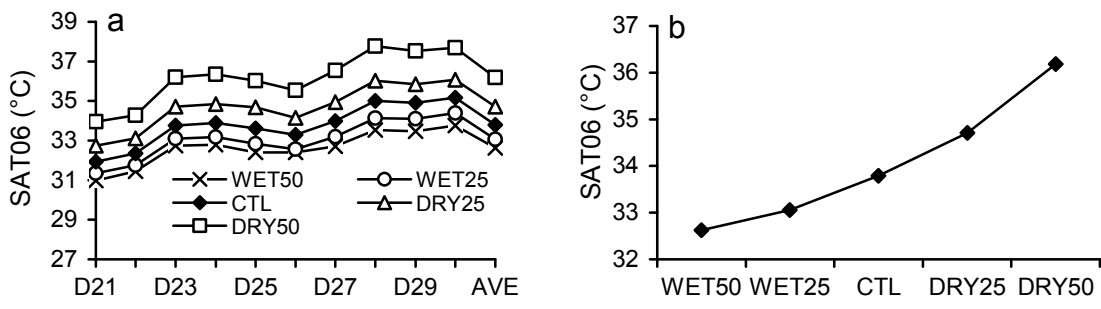
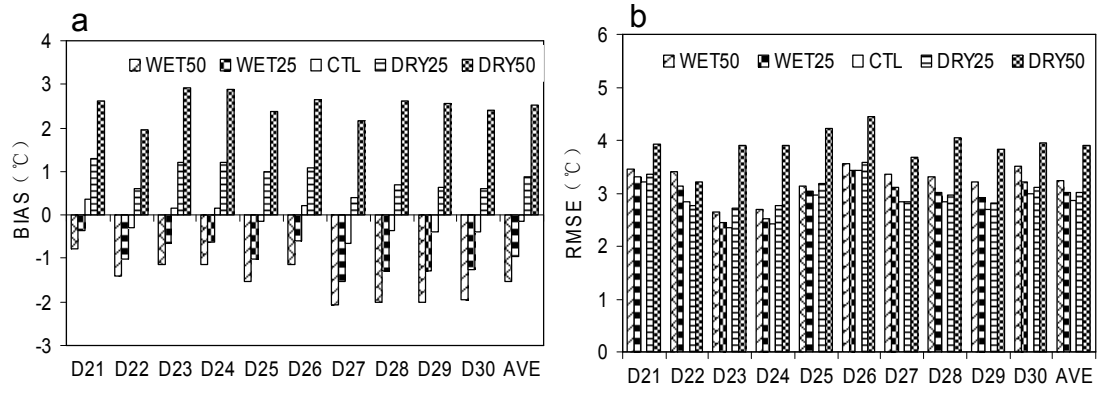


Fig. 4. The average SAT06 values for area D3 in the simulations. (a) The values as changed with the individual simulations with an average (AVE) for each group of simulations. (b) The ten-day means as changed with the five groups of simulations.

1
2
3
4
5
6
7



8
9
10
11
12
13
14
15
16
17
18
19
20
21

Fig. 5. The BIAS (a) and RMSE (b) values for SAT06 in the individual simulations with a ten-day average (AVE).

1
2
3
4
5
6
7
8
9
10
11
12
13

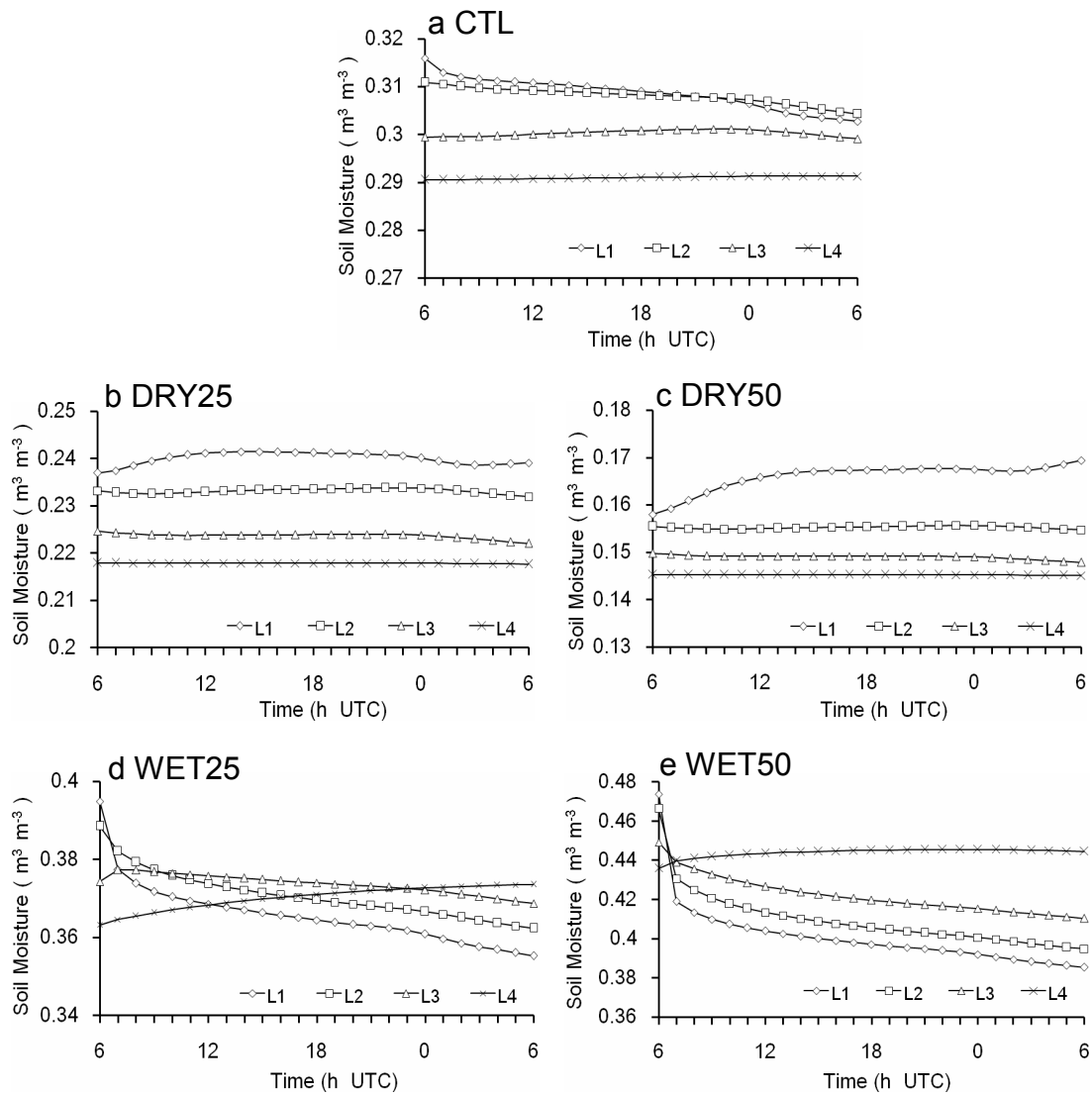


Fig. 6. The mean hourly variations in soil moisture (unit: $\text{m}^3 \text{m}^{-3}$) in the five groups of 24-hour simulations for 20–29 July 2003, where L1, L2, L3 and L4 represent 10-, 30-, 60- and 100-cm-thick soil layers, respectively.

1
2
3
4
5
6
7
8
9

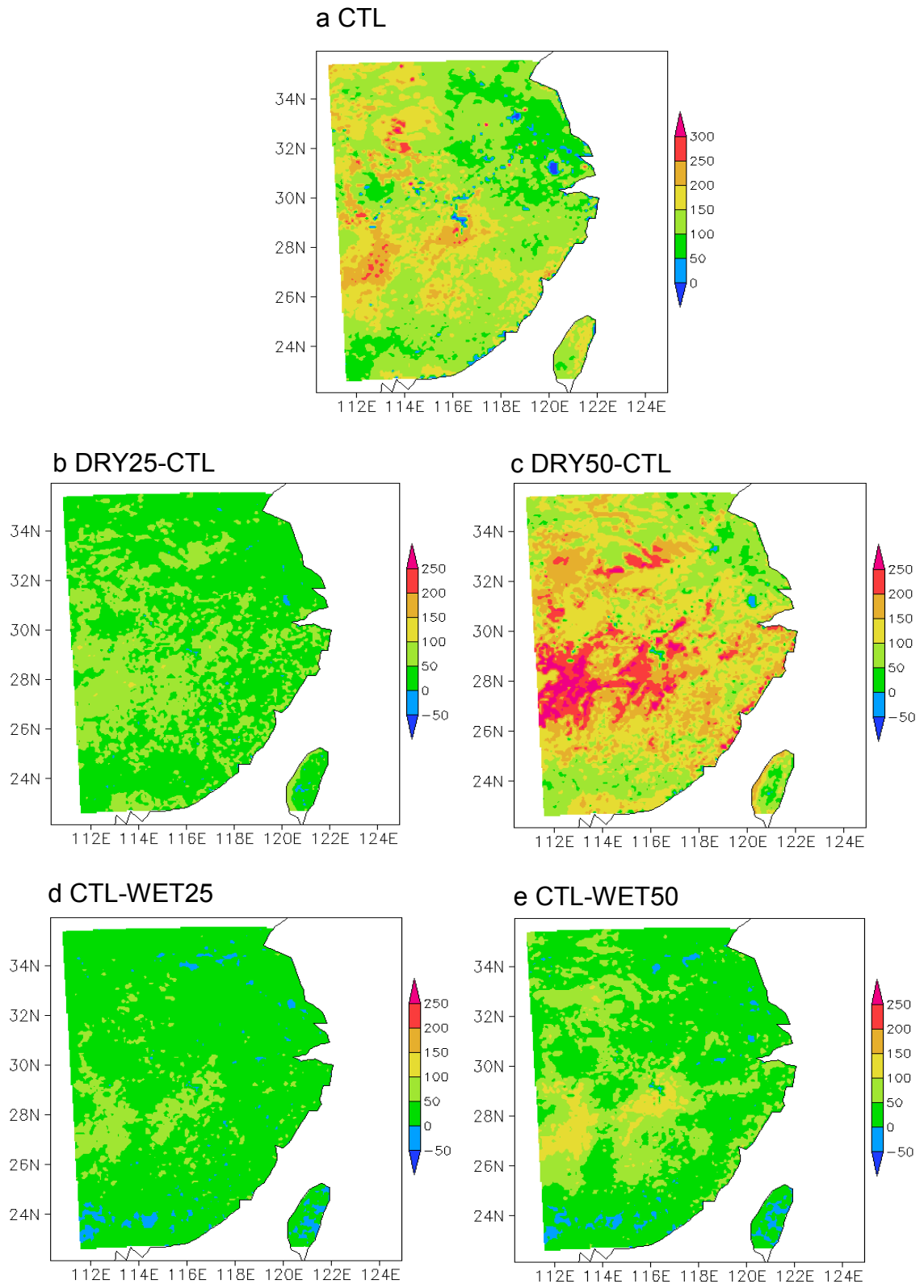


Fig. 7. The spatial distributions of the ten-day mean 0600 UTC sensible heat fluxes in the simulations (unit: $W m^{-2}$).

1
2
3
4
5
6
7
8
9

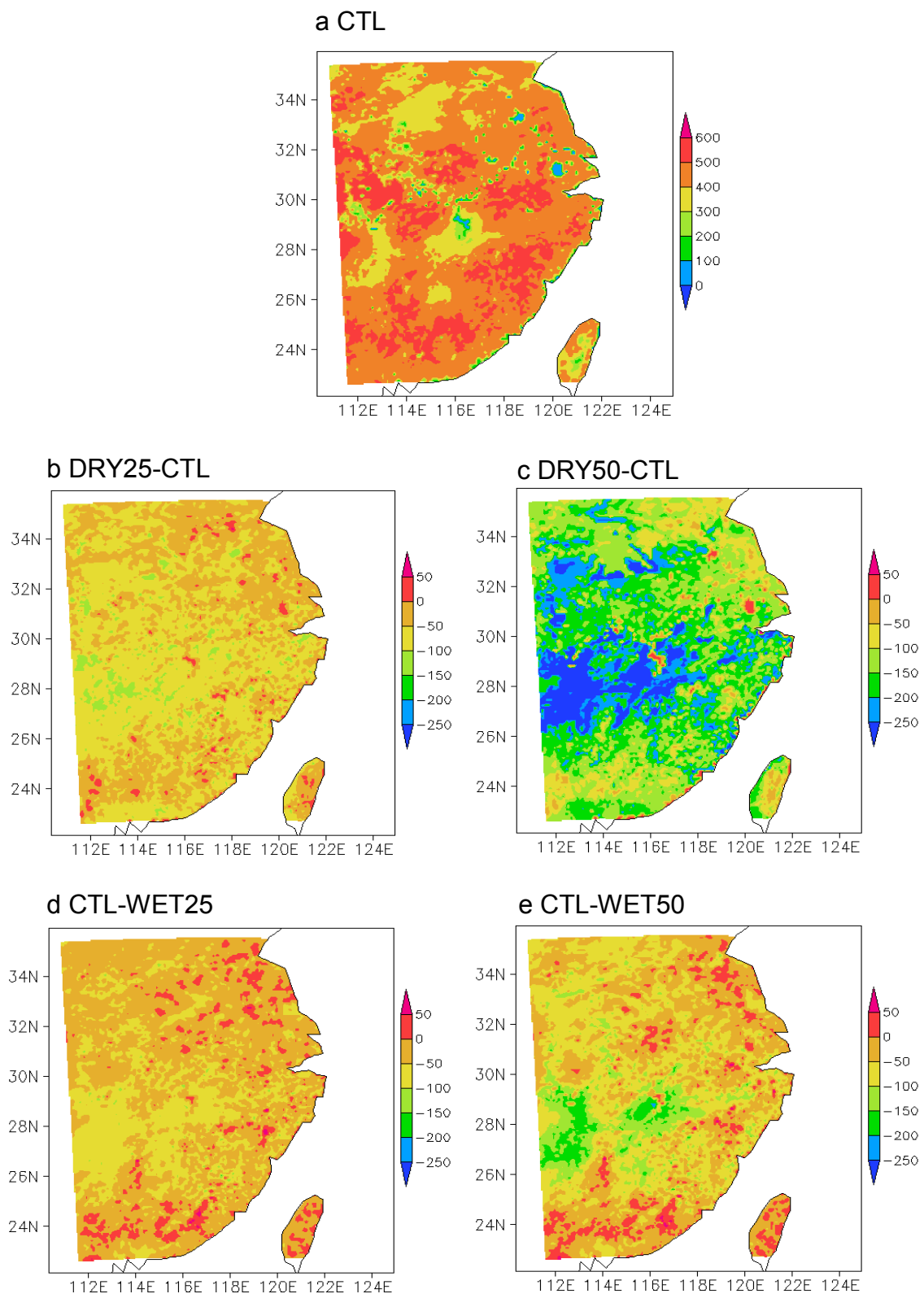


Fig. 8. Same as Fig. 7 but for latent heat fluxes.

1
2
3
4
5
6
7
8
9
10
11
12
13
14
15
16
17
18
19
20
21
22
23
24
25
26

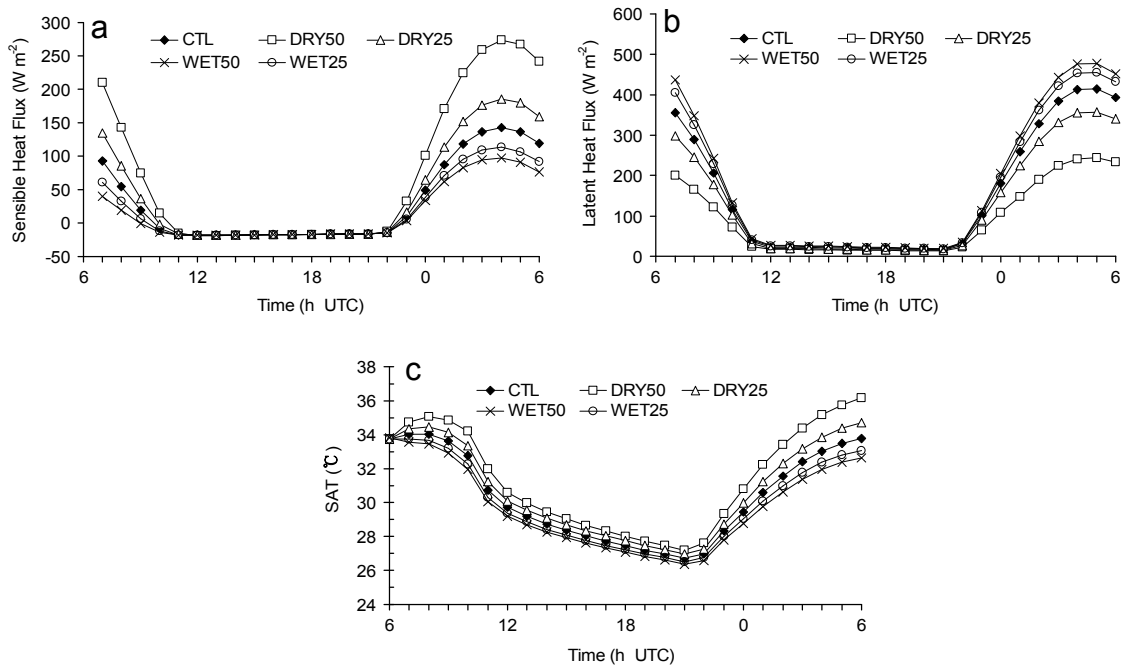


Fig. 9. The mean hourly variations in the area-averaged (area D3) surface quantities for the five groups of simulations during 20–29 July 2003, where the initial flux values are zero (not shown) and the initial temperatures are the same value. (a) Sensible heat flux. (b) Latent heat flux. (c) SAT.

1
2
3
4
5
6
7
8
9

15
16
17
18
19
20
21
22
23
24
25
26
27

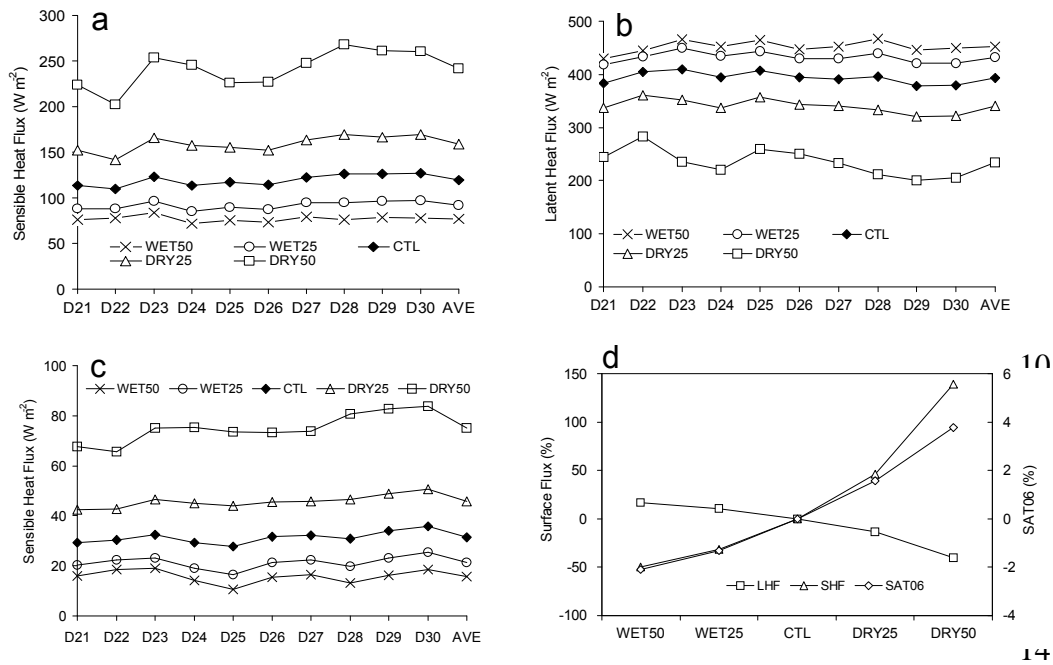
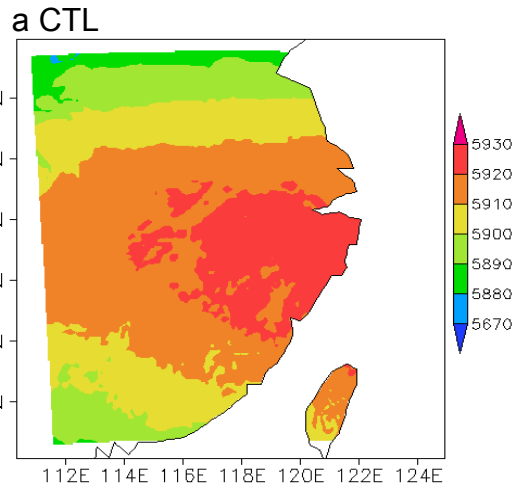


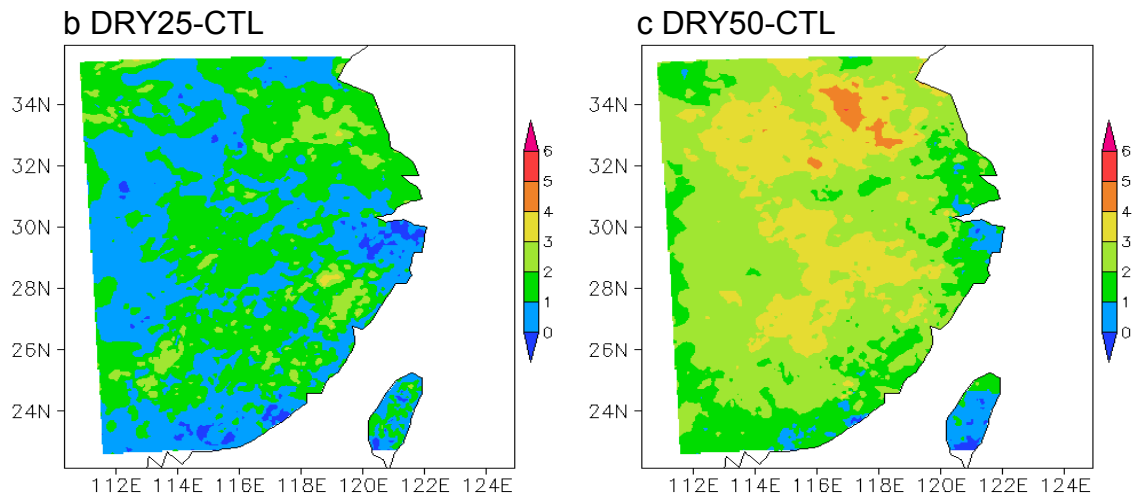
Fig. 10. The area-averaged sensible and latent heat fluxes and SAT06. (a) The 0600 UTC sensible heat flux for individual simulations with a ten-day average (AVE) for each group of simulations. (b) The same as (a) but for latent heat flux. (c) The same as (a) but for the 24-hour mean sensible heat flux (SHF). (d) The relative differences (%) in the ten-day mean 24-hour-averaged sensible heat flux (SHF), latent heat flux (LHF) and SAT06 compared to CTL.

1



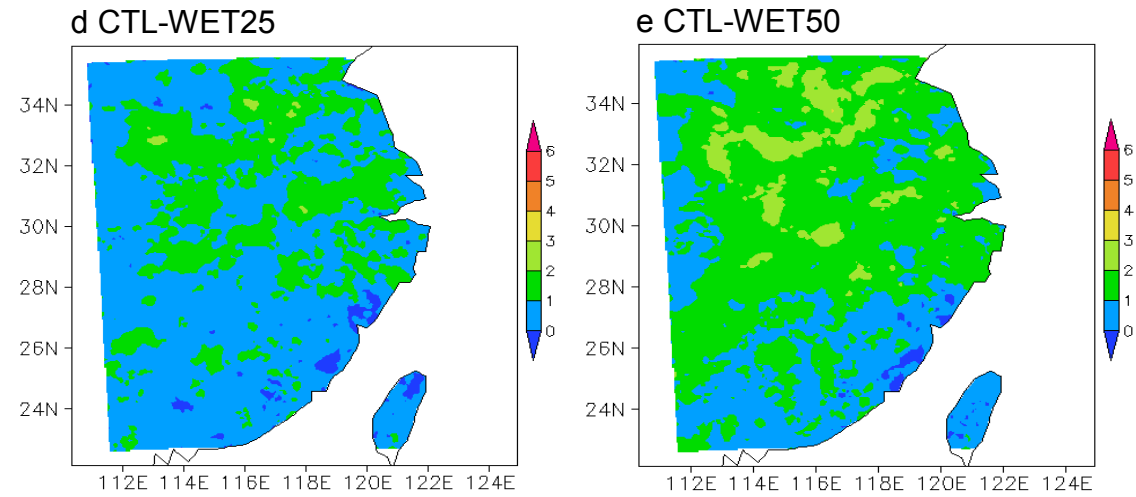
2

3



4

5



6

7

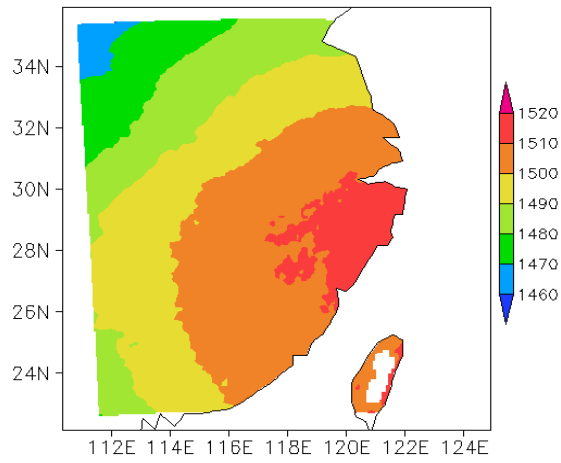
8 **Fig. 11.** The ten-day mean 0600-UTC 500-hPa geopotential height fields and the soil
9 moisture-induced differences in the five groups of simulations (unit: gpm).

10

1

2

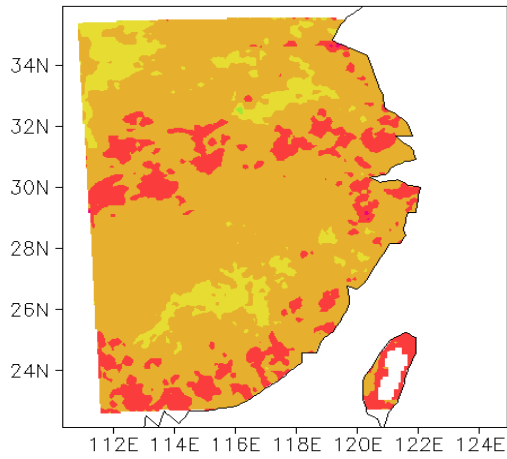
a CTL



3

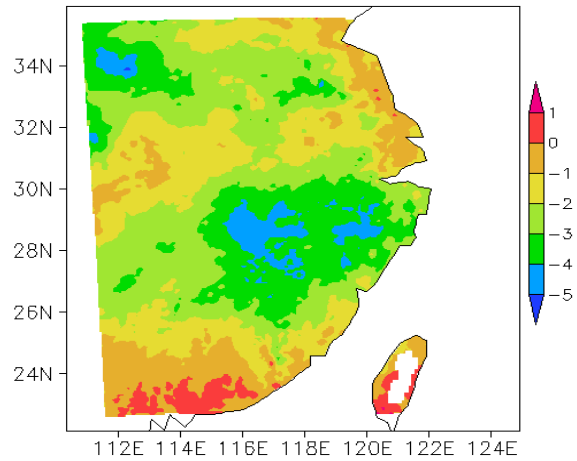
4

b DRY25-CTL



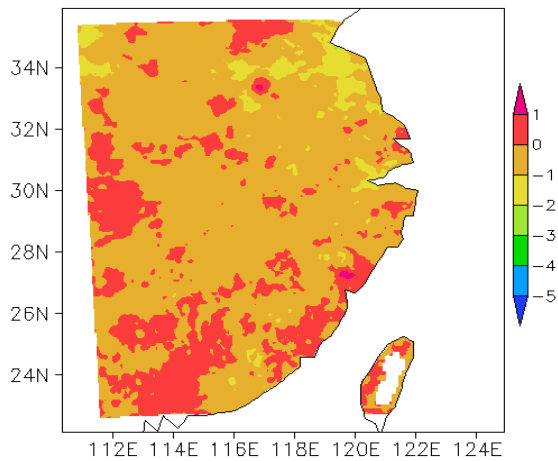
5

c DRY50-CTL



6

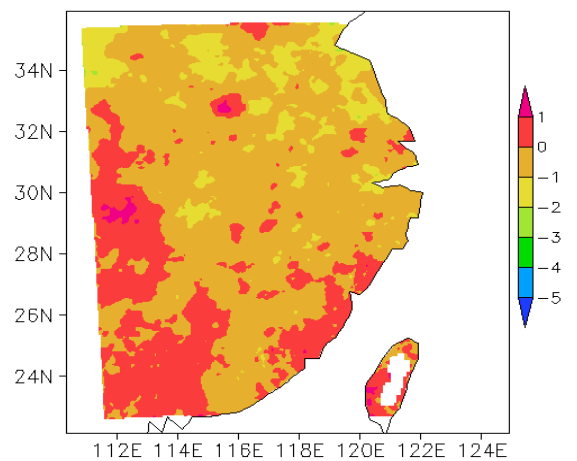
d CTL-WET25



7

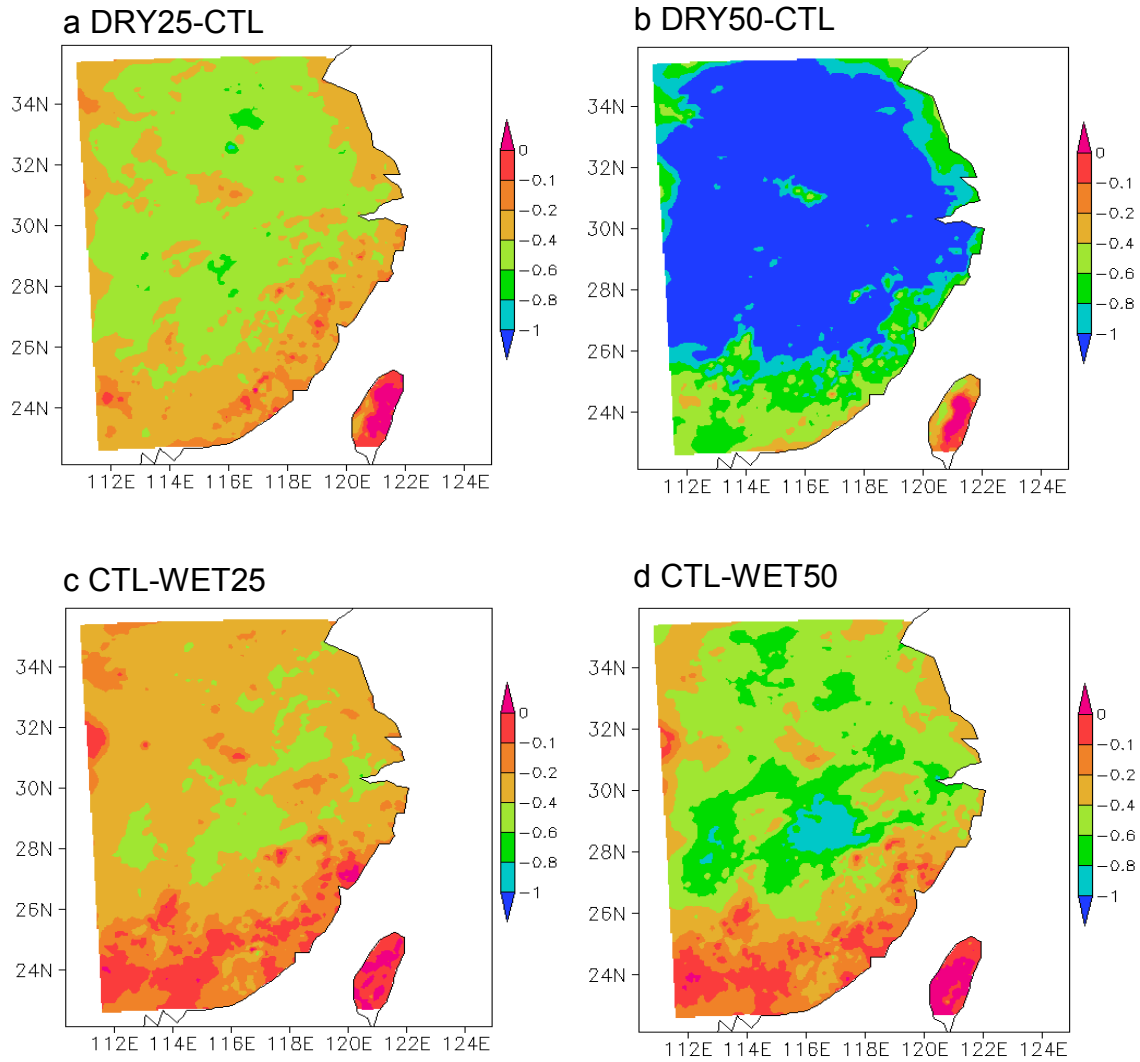
8

e CTL-WET50



9 **Fig. 12.** Same as Fig. 11 but for 850 hPa.

1
2
3
4
5



6
7
8
9

10 **Fig. 13.** The ten-day mean 0600-UTC surface pressure difference fields as compared between
11 different groups of simulations (unit: hPa).

12
13
14

1
2
3
4
5
6
7
8
9
10
11
12
13
14
15
16
17
18
19

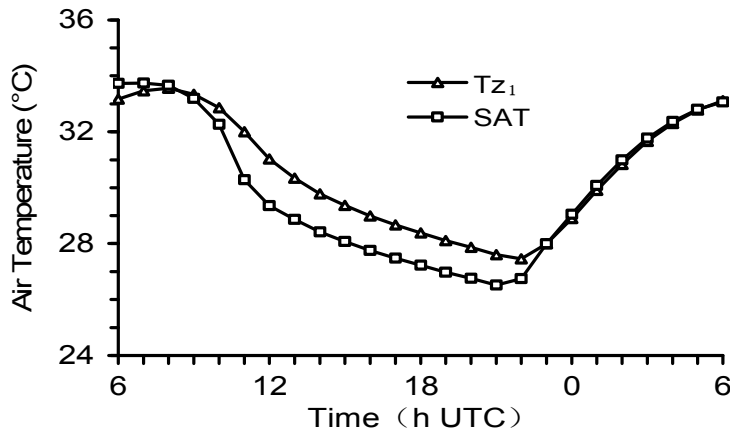


Fig. 14. The mean hourly variations of 2-m air temperature (SAT) and the air temperature at the lowest model level (T_{z1}) in the CTL run for 20–29 July 2003.